To Study the Effect of Reinforcements on the Mechanical and Corrosion Behavior of Electrodeposited Ni-W-P Ternary Alloy Coatings

By

Humaira Kousar

School of Chemical and Materials Engineering

National University of Sciences and Technology

May, 2022

To Study the Effect of Reinforcements on the Mechanical and Corrosion Behavior of Electrodeposited Ni-W-P Ternary Alloy Coatings

Humaira Kousar

Reg. No: NUST2018 MSE13-00000273750

This thesis is submitted as a partial fulfillment of the requirements for the degree of

MS in (Materials and Surface Engineering)

Supervisor Name: Dr. Malik Adeel Umer

School of Chemical and Materials Engineering (SCME)

National University of Sciences and Technology (NUST)

H-12 Islamabad, Pakistan

May, 2022

DEDICATION

I dedicate this thesis to my loving and caring mother, my beloved father, my brothers and my sisters.

Acknowledgements

In the name of ALLAH, the most merciful, the most beneficent.

All praises to Allah Almighty who is the creator of this world and beyond. Uncountable salutation to His best messenger Muhammad (peace be upon him), who ordained us to get knowledge from cradle to grave. As Allah says in the Holy Quran:

“Read! In the name of your Lord” (Alaq, the first revealed ayah)

I express my appreciation and respect to my supervisor Dr. Adeel Umar for his invaluable supervision, proficient guidance, inspiring motivation, generous support, help and conservative criticism that helped me to complete this long-awaited project and thesis. I am thankful to Dr. Muhammad Shahid, Dr. Sofia Javed and Dr. Farhan Javaid for their insightful suggestions and optimistic attitude. I’m grateful to HOD and Principal for providing me research facilities and to all faculty members who helped me to complete my MS degree and to all lab engineers for their help in technical guidance.

I acknowledge the dedication and help of Mr. Khurram Shehzad and Mr. Kashif Mehmood, during my research. Last, but not the least, I want to thank my family for their prayers, support and confidence on me without which I would not have been able to reach my full potential.

Humaira Kousar

Abstract

Ni-W-P based coatings offer promising properties such as superior hardness, wear resistance and high corrosion resistance. The emphasis of this evaluation has been put on improvement of mechanical and corrosion resistant properties of Ni-W-P by inclusion of the suitable BN and Al_2O_3 nanoparticles loading along with deposition. Ternary Ni-W-P alloy coating and both composite coatings (Ni-W-P/Al_2O_3 and Ni-W-P/BN) with particles concentration of (0.1g/L, 0.2g/L, 0.4g/L, and 0.8g/L) were successfully deposited on HSLA steel substrates via electrodeposition method. Their mechanical and corrosion resistant properties were studied using SEM, EDS, nano-indentation, optical profilometry, wear and corrosion tests and comparison was made. Addition of nano Al_2O_3 particles led to an enhancement in mechanical properties while addition of BN reduces the FC and wear rate of the coatings significantly. Corrosion rate when compared with HSLA steel decreased considerably but remained almost the same for BN and nano-alumina loadings. The hardness value of Ni-W-P (0.2g/L) alumina and Ni-W-P (0.8g/L) BN when compared to Ni-W-P alloy coatings increased from 8.84 to 11.60 GPa and 10.83 GPa respectively, the wear rate decreased from 1.834×10^{-7} to 1.946×10^{-8} (mm^3/m) for (0.2g/L) alumina and for (0.8g/L) BN it decreased to 6.634×10^{-10} (mm^3/m). Corrosion rate also decreased from 2.82 to 1.54 and 1.46 mils/yr for alumina and BN loadings respectively. It is concluded that concentration of 0.2g/L of alumina in Ni-W-P composite coating displayed better mechanical and corrosion resistant properties while Ni-W-P/BN (0.8g/L) reported superior wear resistant properties.

Table of Contents

List of Figures

List of Tables

List of Abbreviations

NACE	National Association of Corrosion Engineers
EU	European Union
HSLA	High Strength Low Alloy
Cr	Chromium
Ni	Nickel
W	Tungsten
P	Phosphorous
Al_2O_3	Alumina
wt%	Weight percent
SEM	Scanning Electron Microscopy
EDX	Energy Dispersive X-ray
AFM	Atomic Force Microscopy
HV	Vickers hardness
GPa	Gega Pascale
FC	Friction Coefficient
PP	Potentiodynamic Polarization

Chapter 1

Introduction

NACE international in March 8, 2016 reported the global annual cost of corrosion as 2.5 trillion dollars for iron and steel. This cost increases day by day because of the corrosion and erosion of metal present anywhere inside or outside the homes especially in the aggressive environments like oil and gas industries, sulfuric acid plants, petroleum industries, automobiles (gears, radiators, and fuel and exhaust systems), geysers, aerospace and bridges etc.[1]. For this reason, surface engineering through advance coating materials is the robust method to protect the metallic surfaces of base metals like iron, steel and their alloys. HSLA steel because of its high strength and toughness has been used in automobile, oil and gas and aerospace industries. So it must need to be protected against aggressive outer environments such as high temperature, erosion and corrosion.

Detailed studies shown that the electrodeposited binary alloy Ni-P coating exhibit distinct properties depending upon phosphorous content, electroplating bath composition, plating conditions and post-treatment. These deposits have shown good mechanical properties, favorable tribological features, thermal stability, high corrosion and wear resistant properties, excellent electrical and electrocatalytic activity. The application of Ni-P alloy coatings can be found in automotive, aerospace, and general engineering industries. Notably these coatings are used for protective and functional applications for instance under layer of magnetic disk and thin film resistors [2] [3]. They are also used as a coating in high precision components, thin film magnetic memory discs, diffusion barriers, micro batteries and sensors [4] [5]. This Ni-P alloy coating is a good and promising substitute to the hard chromium coatings which has excellent properties as described above except that its electrolyte contains toxic hexavalent Cr(VI) ions during its preparation and is banned by EU directives (2000/53/WE, 2011/37/UE) [6].

Electroplating is considered one of the useful techniques for making thin and thick surfaces. Electrodeposition technique has several advantages over a lot of deposition processes as it provides high deposition rates, compact, dense, homogeneous, well adhered and thick layer coatings possible in a relatively short time, requires very low

temperatures hence less consumption of energy and are environmental friendly [7]. To further enhance the mechanical and corrosion resistant properties, another metallic element such as Ni, Cu, W, Co, Fe, Sn, Mo [8] etc. can be co-deposited with Ni-P matrix. Tungsten has distinct properties which includes high hardens, high tensile strength, high melting point, low coefficient of linear thermal expansion etc. and have attracted attention of lot of researchers in fabricating ternary Ni-W-P alloy coatings [9] [10] [11] [3]. Tungsten is used in a variety of applications such as glass technology, cut ends, military armor, drills, lathe pens and milling tools, refractory materials and guides etc [8]. Tungsten, a refractory metal, can't be deposited alone from any aqueous solution, but with iron group transition metals it can readily be deposited from the aqueous electrolyte containing tungstate ions ($NaWO_4$) [12]. Hence, addition of tungsten in electrodeposited Ni-P matrix can improve properties like wear resistance, high hardness [12], thermal stability [13], corrosion resistance [14] and electrical resistance and strength. Mechanical and corrosion resistant properties of Ni-W-P alloy can further be enhanced with reinforcement of hard or soft ceramic particles depending upon the applications. For this purpose different particles were utilized for instance BN [15], CNTs [16], CNFs, SiC [17], ZrO_2, TiO_2 [18] and CeO_2 etc.[19].

1.1 Advance Surface Coating Techniques

In the era of advanced materials and surface engineering, different techniques have been utilized in order to enhance and sometimes repair or modify the surface of the base metal. For this purpose there are several techniques which include sputtering [20], molecular beam epitaxy (MBE) [21], thermal spray coatings which includes physical vapor deposition (PVD) [22], chemical vapor deposition (CVD) [23], plasma spray coatings [24], high velocity oxy-fuel HVOF [25], arc and flame spraying [26] and by a chemical route the deposition takes place through sol-gel method [27], electroless deposition [28] and last but not the least electrodeposition is one of them.

1.2 Electrodeposition Advantages

This technique has many advantages over all deposition methods for instance it provides high deposition rates, compact, dense, homogeneous, well adhered and thick layer coatings possible in a relatively short time, requires very low temperatures hence less consumption of energy and are environmental friendly [29] wide range of

materials and compositions (pure metals, composites and alloys) can be coated through this method with relatively less grain sizes i.e. below 100nm. This technique has few size and shape limitations [30] and gives high hardness and mechanical strengths to the materials, the simplicity of the process, economic viability and extensive scalability also comes under its advantages. It's the bottom up approach where the deposition takes place atom by atom from nanometer scale to millimeter scale.

1.3 HSLA Steel

High strength low alloy (HSLA) steel is a steel that comes under the category of microalloyed steel because it contains a very small amount of vanadium, titanium or niobium which is usually less than 0.15wt%. Its microstructures and properties are highly dependent upon the way they are rolled either in a controlled way at low temperatures or hot-rolled at high temperatures. Such microalloyed steels have yield strengths of around 275 MPa and hence termed as high-strength, low-alloy steels. HSLA steel is very essential steel and has been used in automobile, aerospace and oil and gas industries due to its superior properties like high strength and toughness, formability and good weldability and has a higher strength to weight ratio when compared to low carbon steel [31] [32]. In many of the applications, they are used as a base metal/structure like vehicle frames, onshore and offshore platforms, bridges, chemical industry storage tanks, earth moving and mining equipment [33], oil and gas transmission platforms and aerospace structures where HSLA steel confronts/experiences extreme environments which are mechanical, thermal and corrosive in nature [34]. For this reason, its surface must be engineered and protected against these environments by applying mechanical (high strength and hardness) and corrosion resistant coatings.

Figure 1.1. HSLA microstructure and its products

1.4 Different Techniques of Electrochemical Deposition

There are different techniques of electrochemical deposition namely electroless deposition, electroforming, electrodeposition which includes direct current, pulse current and pulse reversed current, and laser enhanced deposition.

Electrodeposition

Electrodeposition, sometimes also called electroplating; is a surface modification technique in which a deposition of a metal takes place electrochemically from its electro-bath containing ions on the conductive materials. For this process two electrodes namely anode (counter electrode) and the cathode (working electrode) are immersed in order to carry the current from the electrolyte and to complete the circuit. These electrodes are connected to the external battery providing an AC current and hence forms a complete electrochemical cell. The deposition baths also called electrolytes are usually prepared by dissolving metallic salts which contains positive as well as negative ions.

With the application of external voltage, the electronic current flows between the two electrodes and the charges species move from one electrode to another carrying out migration and diffusion towards electrode surface which get polarized. The deposition

process occurs only when the conduction mechanism changes from ionic to electronic at the electrode's interface of where electrochemical reactions took place which promotes the redox reactions of the ionic species [35]. Oxidation reactions (loss of hydrogen or electrons) takes place at anode and reduction reactions (gain of hydrogen or electrons) takes place at cathode. As these two reactions takes place simultaneously, hence they together are called redox reactions. The general electrochemical reactions are as follows:

Reaction at Anode: $M \longrightarrow M^{n+} + ne^-$

Reaction at Cathode: $M^{n+} + ne^- \longrightarrow M$

Where M denotes any metal, M^{n+} denotes metallic ion formed in an electrolyte and ne^- denotes the number of electrons present in the electrolyte.

Factors Affecting Plating Process:

There are many factors that affect the metal deposition or the electrodeposition process which are current density, pH, bath temperature and its composition, agitation speed, addition agents and the impurities (if any) in the electrolyte, physical and chemical conditions of the substrate surface, power supply current waveform and the nature of anions and cations present in the electrolyte. [36]

Electroplating Applications

Electroplating is fundamental to many industrial applications which can be grouped in four categories. **Decorations** (jewelry, watches, water-tap and tableware and furniture fitting etc.), **protection** (domestic appliances, screws, electrical components such as MEMS, hard disk drives and circuit boards etc.), **electroforming** (manufacturing of screens, record stampers, molds and dies, sieves, and dry shaver heads etc.) and **enhancement** (to improve thermal and electrical conductivity, reflectivity, electrical contacts, solderability, micro-parts production for MEMS) [37].

1.5 Nickel and Nickel Binary Alloy Coatings:

Nickel coatings have been deposited via different production techniques and electrodeposition is one of them. Nickel is a very important and versatile metal for

decorative and engineering purposes and have a very prominent role in metallurgy. It has been utilized and electroplated in different applications which includes from very simple thin films; either for decorative purposes or for functionally suitable metal coatings/surface engineering purposes (corrosion and wear resistant coatings) to bulk and complex electroforming products for instance rotatory printer cylinders. Nickel coatings promises a unique combination of providing hard, bright and lustrous appearance, compact, wear and corrosion resistant coatings such as transport and service apparatus [38] and for such properties it gained immense popularity [39]. Nickel coatings; because of their excellent adhesion properties, are often used as an undercoat in chrome plating. Although nickel plating is done and is widely used for centuries and is well advanced in its optimized plating parameters but still there exists considerable interests and need for improving its mechanical and corrosion properties which are highly influenced by plating bath compositions and parameters. [30] For this purpose many researchers have employed binary alloyed as well as composite coatings which includes Ni-X (X= B[39], P [40], W [41], Co [42], Cu [43], Mo [44] and CNTs, BN, Al_2O_3) respectively. Different electrolytic baths for deposition of nickel have been reported by researchers some of which are acetate bath [45], lactate bath [45], sulphamate bath [46], chloride bath [47], bath having gluconate salts [30] and citrate baths [48]. Nickel coatings are widely applied to steel structures for their protection from abrasion and corrosion.

Figure 1.2. Nickel and its alloys

1.6 Nickel Ternary Alloy and Composite Coatings:

To enhance the mechanical and corrosion resistant properties of the Ni-binary alloy coatings even further, researchers develop their interest and become more inclined towards the Ni-ternary alloy coatings which include Ni-B-P, Ni-P-Co, Ni-P-Cu, Ni-P-Co, Ni-P-W and sometimes with Ni-ternary alloy, they studied rigorously the behavior and properties of different reinforced particles of different sizes and types which results in composite coatings. The performance of composite coatings exceeds the conventional coatings which are highly in demand for industrial purposes and are more likely to perform well in extreme environments like temperature, fatigue, corrosion, erosion, abrasion and friction. [49] For this purpose different particles were utilized for instance BN, CNTs, Al_2O_3, CNFs, SiC, ZrO_2, TiO_2, and CeO_2 etc.

Mechanical and corrosion resistant properties of Ni-P-W alloy can further be enhanced with reinforcement of hard or soft ceramic particles depending upon the applications. For this purpose, different particles were utilized for instance BN, CNTs, CNFs, SiC, ZrO_2, TiO_2, and CeO_2 etc.

1.7 Materials Used

Nickel

Nickel is a metal which lies in the 10^{th} group of the periodic table, has a face centered cubic (FCC) structure with five stable isotopes and is tough and harder than iron. Baron Axel Fredrik Cronstedt in 1751 isolated nickel for the first time and classified it as a chemical element. It's melting and boiling points are 1455°C and 2730°C respectively. Nickel is used in many industrial and consumer products for instance rechargeable batteries, stainless steel and cast irons (to increase tensile strength, toughness and elastic limit), coinage, alnico magnets, and some special alloys such as permalloy, elinvar and invar.

Tungsten

Tungsten is a strong refectory metal belongs to the group 6; was first isolated by Spanish chemist and mineralogist Juan Jose and Fausto Elhuyar by the reduction of WO_3 which is derived from the mineral wolframite. That is why it's also called wolfram. It has the atomic number 24, atomic weight 183.85, density 19.3grams/cm^3 at 20°C, melting and boiling points as 3410°C and 5660°C respectively. It is mostly used in steels to increase their hardness and strength. In nickel matrix its key role is to provide solid solution strengthening [50].

Phosphorous

Phosphorous belongs to the 15^{th} group of periodic table and is discovered by Hennig Brand in 1669. In the earth's crust, phosphorus is found to be the 12^{th} most abundant element. Chemically it is extremely reactive, and for this reason it occurs in the form of phosphate ion and hence as phosphate salts. In nickel based alloys, a minor amount of phosphorous provides good creep performance in commercial cast and wrought superalloys [51]. Also, when annealed, precipitation of Ni_3P provides grain refinement which is important in increasing the hardness of the material.

1.8 Aims and Objectives:

In this research the electrodeposition technique is discussed and Ni-W-P alloy, Ni-W-P/Al_2O_3 and Ni-W-P/BN composite coatings have been fabricated on HSLA steel. The key objectives of this research are:

1. To find out the coating material that has great performance regarding mechanical and corrosion properties after doing extended literature review.
2. To choose best combination of materials for ternary alloy electrodeposition, to optimize bath parameters and to choose substrate for research work.
3. To successfully deposit Ni-W-P alloy, Ni-W-P/Al_2O_3 and Ni-W-P/BN composite coatings via electrodeposition method on HSLA steel.
4. To examine the structure, morphology, roughness, hardness and elastic modulus, corrosion and wear resistant properties and their discussion. Also, to study the effect of different alumina and BN concentration on above mentioned properties.

1.9 Overall Dissertation Outline

This thesis contains five chapters whereas the first chapter introduces the work containing the background and objectives. The second chapter comprised of literature review. It contains review of binary and ternary coatings and also different kind of inclusions that researchers had added in their coatings. The third chapter elaborates the work methodologies and experimental procedure which are briefly explained step by step. Also, it includes a short introduction to characterization techniques which has been utilized to analyze alloy and composite coatings. In chapter four, all the results have been discussed extensively that were taken during the whole research. This chapter also draws the comparison of mechanical and corrosion resistant properties between Ni-W-P/Al_2O_3 and Ni-W-P/BN composite coatings. Chapter five draws the conclusion of the whole work and contains the recommendation for the future work. Chapter six is the last chapter which contains all the references that were used for the understanding the concepts and thesis write up.

Chapter 2

Literature Review

This chapter briefly explain the literature survey on the topic "To study the effect of alumina in electrodeposited Ni-W-P ternary alloy coatings and its mechanical and corrosion resistant properties". It includes different binary and ternary alloy coatings with different type of inclusions and their relative discussion done by researchers.

2.1 Ni-P-W Coatings

Supriyo Roy et al [52] used the mild steel (AISI 1040) as a substrate to study the behavior of Ni-P-W coatings via electroless method. Bath chemicals were used in a way that the source of nickel is provided by nickel sulphate. Sodium hypophosphite functions as a reducing agent and sodium citrate functions as a complexing agent. The lactic acid was also used as a stabilizer in the electrolyte. The thickness of the coating was found to be 20-25 microns. The composition of the coatings through EDX analysis came out to be 88.57% Ni, 7.62% P and 3.81% W. Through SEM micrographs, the morphology of the coatings was seemed to be globular; distributed randomly and had low porosity with optically smooth and dense surface. The average roughness of coatings got increased by 0.08 microns when compared with the substrate without coating and it reached the value of 0.48 microns. It is also reported that with the increased in tungsten concentration, the roughness and hardness of the coatings also increased i.e. when tungsten content is above 40wt%, the hardness becomes greater when compared to substrate. This is due to the phenomena of solid solution strengthening and phosphide precipitation, thus improving thermal stability of as deposited Ni-P-W coatings.

Jinku yu et al [9] observed the effects of sodium hypophosphite on the properties of Ni-P-W coatings via electrodeposition method on copper sheets as a substrate. The bath had the composition of 15-25 g/L $NiSO_4.6H_2O$ nickel sulphate hexahydrate, 60-80 g/L $Na_2WO_4.2H_2O$ sodium tungstate, 4-12 g/L $NaH_2PO_2.H_2O$ sodium hypophosphite, 40 g/L H_3BO_3 boric acid, 80 g/L $Na_3C_6H_5O_7.2H_2O$ tri-sodium citrate, and 5 g/L saccharin (which is used as a brighter and stress removal agent). XRD results

depicted the transformation of morphology from nanocrystalline to amorphous when the concentration of sodium hypophosphite increases above 8g/L. DSC curves revealed the exothermic peaks of Ni-P and Ni-P-W alloy at 337.8 and 431.6K respectively, indicating the phase transition in the structure. The deposition rate firstly increases with increase in concentration of sodium hypophosphite from 4 to 10g/L and then decreases. Also as the current efficiency of phosphorus increase, it decreases for tungsten during the process. The total decrease in current efficiency from 33.10 to 27.80% was reported. The influence of sodium hypophosphite on phosphorus and tungsten content in Ni-P-W alloy coatings was also studied. It showed that the tungsten content decreases with the increment in sodium hypophosphite and on contrary the P content increases. It is reported that the SEM images of Ni-P-W alloy coatings showed uniform, dense, porous or crackles coatings with fine and smooth spherical nodular structure. The grain size of the coatings significantly decreases with the increase in concentration of sodium hypophosphite from 4 to 12g/L. The maximum hardness is achieved with 6g/L sodium hypophosphite and reached the value of 663.7HV. Another imperative study is also revealed that with the increase in sodium hypophosphite, the corrosion resistance of the coatings increases.

Mara Cristina Lopes de Oliveira et al [10] deployed electroless method to deposit Ni-W-P coatings and studied the influence or behavior of different tungsten content using SEA 1020 carbon steel. The vital study reported here is that the pH of the bath is optimized to 9 where charge transfer resistance becomes low. XRD was conducted which revealed two main peaks at 44.5° and 51.8° corresponding to Ni (111) and Ni (200) planes. XRD of the annealed samples showed different reflections attributed to Ni_3P phase and these phases originate from temperature 350 to 500°C. EDS results revealed the phosphorous content ranging from 6 to 10wt% for the baths 1 to 4 but for the bath 5 (bath compositions can be seen from the paper) it showed lower P content than 6wt% indicating low phosphorous coatings. The reason for low phosphorus deposits as tungsten is added was due to the increase in metallic ions to hypophosphite ratio in the bath. Thickness of the coatings was analyzed via SEM and it revealed the homogeneous coatings for all the baths and the thinnest of all i.e. 14.60 ± 1.39 mm was obtained from the bath 5, indicating that with the highest tungsten concentration, the deposition rate decreases. SEM also revealed that for the bath one with no tungsten content, the morphology was smooth with some small cavities, but as the tungsten

content enhances, the morphology becomes more and more nodular from bath 2 to 5 and their size also gets increased giving rise to a smoother surface. Nanoindentation test revealed that the hardness of coatings increases as the tungsten amount increases and it further increases after annealing at 400°C for 1 hour and this is because of Ni_3P crystallites in the nickel matrix. CLSM 3D images indicates a relatively smooth topography with respect to bath 1 with no tungsten content, as it's been observed that the tungsten increment reduces the film roughness. Potentiodynamic polarization test revealed that the corrosion current density (i_{corr}) is decreased for all the coatings and the corrosion potential (E_{corr}) values shifted towards nobler values when compared with the bare uncoated steel. The best values for E_{corr} and i_{corr} were obtained from the bath 5 which were -177(mV) and 0.53($\mu A.cm^{-2}$) respectively.

Abhijit Biswas et al [53] investigated the wear behavior of Ni-W-P coatings in before and after phase transformation period. They utilized electroless coating technique for the Ni-W-P alloy deposition on low alloy steel (AISI 1040). EDX revealed their weight percentages of nickel around 83.10 %, phosphorous as 11.68wt% and tungsten as 5.22wt%. SEM images revealed that the alloy coatings exhibit a typical nodular morphology with no porosities and are quite dense. Shiny bright particles appeared on the coatings because of the extra growth of nickel alloy. The average thickness of Ni-P-W alloy coatings came out to be 25μm and had very good bonding with the substrate. DSC plots give sharp exothermic peaks indicating that a immense atomic activity is there which results FCC nickel structure and some of its precipitates with phosphorous known as phosphide Ni_3P, and transforms amorphous structure to crystalline structure. The activation energy for Ni-P-W coatings was evaluated and had the value of 230.28 kJ/mol. XRD was done in order to achieve peak profiles for as- deposited and heat treated Ni-W-P coatings. A broad peak from 40-50° (2θ) was obtained indicating FCC nickel crystallite plane telling amorphous structure. Different peaks were found when deposits were heat treated as 348°C, 400 to 800 °C. Many Ni_3P peaks were also originated at 348°C along with broad Ni peak indicating that Ni_3P phases get precipitated prior to the nickel phase. These phases include Ni (111), Ni_3P, FeP, tungsten nitride oxide W0.62 (N0.62O0.38), NiO, WP, WO_3, W0.62 (N0.62O0.38), Fe_2N peaks were obtained. Morphology also changes with the change in the temperature and SEM images revealed that at 200°C, size of nodules increases as the grain growth occurs. At 348°C PTT, no significant changes were seen, while heated at

400°C, cracks appear and becomes blackish in color when heated at 600°C and finally coatings lost their adhesion with the substrate when heated at 800°C. Maximum hardness of 1130HV was obtained when given a heat treatment for 1 hour at 400°C and highest co-efficient of friction was obtained for as deposited coatings and has the value of ~ 0.31.

Santanu Duari et al [54] studied the mechanical properties especially tribology and friction of electrodeposited Ni-P-W coatings via electroless method under lubricated and dry conditions. The cylindrical mild steel (AISI 1040) was used having the dimension of 6mm diameter and 30mm in length. Table 2 in the article demonstrates the deposition conditions and bath composition of the Ni-P-W coatings. EDX spectrum shows well defined nickel, tungsten and phosphorous peaks confirming their presence in the coatings and their percentages are 84%, 4% and 12% respectively. This reveals that the coatings contain high phosphorous content/range and could have amorphous morphology. XRD revealed that the coatings have both amorphous and crystalline phases and this is because of the settling of tungsten in Ni-P matrix. After annealing the structure becomes more crystalline giving high reflection of Ni peak. SEM indicates nodular morphology of Ni-P-W coatings which are quite homogeneous and non-porous. The coating thickness was around 30μm. Micro Vickers hardness and surface roughness tests were performed showing their direct relation with the wear resistance. Hardness of 678 $HV_{0.5}$ was obtained for as-deposited coatings and on one hour annealing at temperature 400°C, the hardness significantly rises to the value of 994 $HV_{0.5}$.This increase in hardness is due to the formation of hard and stable phases of Ni_3P and the solid solution strengthening due the tungsten. The average roughness of 125 specimens comes out to be 0.9148 μm a bit higher than the average roughness of the substrates i.e. 0.8μm. The tribological behavior of the coatings was studied under lubricated sliding conditions. It was revealed from the results that the wear depth of the track increases with the more load and sliding speed and hence the sliding distance increases leading to higher wear rate.

2.2 Cu-Ni-P/Cu-Ni-P-W Coatings

M. Karunakaran et al [55] used the aluminum substrate of the grade Al-6063 to study the physical properties of ternary Cu-Ni-P and quaternary Cu-Ni-P-W composite

coatings. In their setup, Al-6063 substrate was a cathode and a pure copper as anode. Bath was composed of 250 g/L $NiSO_4.6H_2O$, 15g/L $NiCl_2.6H_2O$, 15 g/L NaCl, 30g/L H_3BO_3, 6g/L H_3PO_4, 80g/L $Na_2WO_4.2H_2O$. SEM Images shows that for the samples coated with Cu-Ni-P have a uniform morphology with fine grain deposits. For Cu-Ni-P-W, the coatings were uniform with crystallized, dense and fine globular structure. From the EDX pattern it is shown that the major portion in the deposited Cu-Ni-P and Cu-Ni-P-W coatings was of nickel. In addition to nickel and phosphorus peaks, the tungsten and copper particles also co-deposited into the matrix. The surface roughness profiles of both Cu-Ni-P and Cu-Ni-P-W were compared and it is revealed that the surface roughness for the former came out to be 1.37μm and for the later it is 2.16μm indicating that the value of surface roughness for Cu-Ni-P-W is considerably high than previous one. This is due to the hard particles of W distributed uniformly into the Ni matrix. The friction and wear performance of the coatings were also studied and then compared. The results clearly exhibits that with more and more inclusion of W particles, the coatings become more resistant to wear and this can be due to the phenomena of solid solution strengthening. Wear rate increases with more amount of W particles. Comparison of wear rate and FOC between Cu-Ni-P-W and Cu-Ni-P coatings on Al indicates low values for the former than the latter. Vickers hardness testing was also performed and indicated the increase in hardness of Cu-Ni-P coatings was due to the decrease in the phosphorous content while the hardness of the Al substrate coated with Cu-Ni-P-W increases with increment of tungsten. The maximum hardness for the latter coatings reached to 470 HV and 153 HV for the former coatings.

2.3 Ni-P-W/CNF's Coatings

A.Akyol et al [8] studied the tribological and corrosion performance of Ni-P-W alloy coatings with carbon nanofiber CNFs as reinforcements through electroless method. CNFs act as solid lubricant in the composites and because of such property they can be used in capacitors, chemical sensors, fuel cells, catalyst supports, gas storage and chemical industry. In their study the aluminum plates were used as a substrate. Three different concentrations of sodium tungstate i.e. 60 g/L, 80 g/L, 100 g/L were used and their properties were compared while the other two concentrations i.e. 0.1 g/L and 0.2 g/L of CNFs were used whereas the concentration of sodium tungstate was optimized and kept constant at 100 g/L. XRD of the samples was done in order to know any

formation of phases and their nature. For the samples W1, W2 and W3, the characteristic peaks were obtained at 44°, 52° and 78°. After receiving heat treatment Ni_3P peaks also observed. Addition of tungsten improved crystallinity and addition of CNFs have significant effect on reduction of grain size of the Ni-P-W deposits. SEM images revealed that the CNF's co-deposited with the ternary alloy, forming nano-composites and increased amount in the bath yield higher content of CNF's in the deposits; which lead to finer grains in the matrix and also homogeneous coatings. In order to know the mechanism of deposition and alignment nature of CNF's in the coatings FESEM was done and it revealed that CNF's surfaces and ends were decorated with ternary alloy and aligned horizontally on the substrate, having low porosity and hence the dense structure. Microhardness of the coatings was also studied which showed that in spite of the dense structure the microhardness of the ternary alloy coatings decreases with the inclusion of CNF's due to inter-channel porosity formation between ternary alloy (Ni-P-W) and the CNF's. However after annealing the microhardness of all coatings increased and the morphology becomes more crystalline and some precipitation of Ni_3P also occurred, reducing the grain size. The highest microhardness of 935HV was obtained with W3 sample after the getting heat treatment at 400°C. The wear resistant of the coatings improved with the addition of CNFs. When the electrochemical corrosion behavior was tested the W3 coating became more corrosion resistant than the other two (W1 and W2) coatings and same is the case with adding CNFs because they behaved as a passive layer.

2.4 Ni-W-Fe Coatings

Aldrighi Luiz M. Oliveira et al [56], through electrodeposition technique fabricated alloy coating of Ni-W-Fe alloy on copper substrate. The effect of increased temperature and current density increases the number of nodules while decreases their size. This is due to the increasing tungsten content in the coatings. It was also observed that as current density increases, no micro-cracks were found in Ni-W-Fe alloy coatings. Also small inclusions of Fe in the alloy transform the surface of coatings into more homogeneous structure and decreases internal stresses of the coatings. XRD results showed wider peaks for Ni-W-Fe alloy representing their amorphous structure. For the experiment 2 and 4 XRD shows broader peaks from 47-41° and 47–38° respectively indicating amorphous structure as bath temperature, tungsten content and

current density increases. Such behavior occurs when number of nodules increases and size of nodules decreases due greater amount of tungsten present in the bath which leads to the amorphous morphology. The effect of tungsten content, current density and temperature was evaluated and it was observed that all these factors have direct effect on the hardness of Ni-W-Fe alloy coatings. Corrosion study was also done through potentiodynamic linear polarization and effect of current density and temperature of electrolytic bath was evaluated and was observed that both of them had positive response and yield better results. This is due to the increased content of tungsten in the electrolyte bath. Also with the increased amount of W, a stable passivation film is formed ranging from -0.306 V to -0.024 V and has the lowest corrosion current density having the value of 8.98 x 10^{-6} mA/cm^2. EIS was also done to ratify any formation of passivation layer, oxide layer, behavior of interfaces and resistance of metals against corrosion. With the help of Nyquist diagram, it was noticed that the polarization resistance of the coating increases and the greatest value of Rp is assigned to the coating with highest tungsten content and this is because of the formation of WO_3 passivation layer. The best polarization resistance came out to be 13,000 ohm/cm^2 and corrosion resistance of the value of 14,041 ohm/cm^2.

2.5 Ni-Sn-P Alloy Coatings

Hongzhi Wang et al [57] used pure copper as a substrate (cathode) and ruthenium titanium anode to deposit Ni-Sn-P alloy coatings via electrodeposition method. Temperature and current density were the varying parameters controlling amount of Sn and P in the alloy coatings. Then because of the excellent corrosion resistance performance, the alloy coatings having the composition 81.39 wt% Ni, 14.56 wt% P, 4.05 wt% Sn, were used for further research. The purpose was to determine the effects of annealing on the properties of Ni-Sn-P alloy coatings. XRD peaks revealed that the as-deposited coatings were amorphous and when annealed at 400 °C, the peaks were still broad indicating that the coatings still possesses amorphous structure. When they were annealed further at 600 °C, it was observed that several small and sharp peaks appeared and indexed to the precipitation of NiP, Ni_3P, Ni_2SnP, Ni_3Sn_4, Ni_2P, Ni_3Sn_2 and SnP_3, hence indicating that the structure transform from amorphous to crystalline. SEM images revealed a smooth, cell-like morphology. A very slight smoothing effect (fine crystal grains) of annealing on the morphology of the Ni-Sn-P alloy coatings was

seen as the temperature changes from 500 °C to 600 °C. The impedance responses of Ni-Sn-P alloy coatings were also analyzed before and after heat treatment and revealed the decrease in impedance values for corrosion reaction as well as in corrosion resistance performance. The RT value also reduces from 2.166 x 10^4 to 4150 Ω cm^2 at 600°C indicating that during annealing, a negative role was played by nitrogen in properties like anti-corrosion for Ni-Sn-P alloy system. Potential polarization measurements were also performed for as deposited and annealed alloy coatings at 600°C. The former shows E_{corr} value of -0.004V and latter shows the value of -0.210V. Similarly the I_{corr} value for former was 11.863μA cm^{-2} and for later was 25.483 μA cm^{-2}. These values indicate that with annealing, coating's resistance become weaker. The SEM images were also taken after corrosion testing of as deposited and annealed Ni-Sn-P alloy coatings and they revealed that uniform corrosion occurred for the former and for the latter it was observed that at 600 °C, the corroded surface was totally rough and uneven and was seriously destroyed.

2.6 Ni-W Coatings

T.Yamasaki et al [58] deposited Ni-W coatings on a copper substrates via electrodeposition method. It is reported that in Ni-W alloy, W content is highly influenced by the ammonium chloride concentration in the deposition baths. When W content becomes high, it leads to crack formation. Amorphous structure of coatings was revealed by TEM. The DTA data shows that the crystallization of Ni-W alloy coatings took place two steps. The first phase of crystallization took place at the temperature of 982K when the precipitates of FCC-Ni-W solid solution forms. The second phase takes place at the temperature of 1100-1150K. XRD results confirms that this is due to the formation of Ni_4W precipitates. The as deposited coatings have hardness of 770HV and when annealed at 673 K for 24 hours, the hardness value raise to the value of 1100HV. When the temperature was further raised to 873K, the structure changes from amorphous to nano-crystalline and the grain size reduces to 12nm which was confirmed with XRD data.

Dmitriy V. Suvoerov et al [59] deposited Ni-W crack free alloy via electrodeposition method using DC and PC modes on copper substrate. In their work, the SEM images revealed that the coatings using DC mode having the pH 8.7, have dense net of micro-

cracks on the surface and they increases as increased in the tungsten content and current density. The width of the coatings came out to be 6 micrometer. Deposits with the pH 9.5, there were no microcracks found and such coatings have pronounced globular structure. Influence of conditions like current density and bath composition on Faradaic efficiency and tungsten content were also studied. The depositions with PC mode and 8.7pH, the Faradaic efficiency decreases up to 20-30%. Higher tungsten content was achieved with the current density ranging 0.03-0.1 Acm^{-2} when compared to DC mode and the reason for that is the decrease in the duty cycles. The X-ray analysis revealed that there is a shift in the peaks when the coatings are produced in PC mode with pH 8.7 and pH 9.5. This is reasoned because of the difference in the lattice spacing and Ni-W compositions both of which depends on the pH of the electrolyte.

Yong-Kwon Ko et al [60] deployed pulse electroplating (PE) technique to deposit Ni-W alloy coatings on copper foil aiming to get crackles coatings. They studied the effects of current density and pulse duty cycle on the Ni-W deposits. They reported that the tungstate ion is only stable at high pH (above 8) and at this pH nickel forms nickel hydroxide, hence for this; a complexing ligand is required and for this they used citrate chemical. The DC source was employed with different current densities and it was studied that with low current densities, there are large pores and their size and number starts decreasing when the current density increases. With the pulse current electroplating at current density of $40mA/cm^2$ they achieved a crackles Ni-W coatings but this cannot be obtained by DC electrodeposition. At the same current density the best surface morphology was obtained. The average hardness of 600HV of the coatings were obtained and the composition of the coatings analyzed by EDS revealed the nickel to tungsten ratio as 4:1.

2.7 Ni-P Coatings

Moo Hong Seo et al [40] studied the effect of phosphorous acid H_3PO_3 concentration on electrochemically deposited Ni-P coatings. For these coatings, alloy 600 plate was used as a substrate. Phosphorous content in the deposits obtaining from sulfamate and sulfate baths was studied. This study shows that from sulfate bath the phosphorous content was readily incorporated in the deposits than sulfamate bath. When the current

efficiency was studied, it revealed that with the increase in H_3PO_3 concentration, the current efficiencies decreases for both types of baths. When the stresses in the deposits were studied, the graphs showed that the stresses in the deposits increases linearly when the concentration of phosphorous acid H_3PO_3 increases for both baths. For sulfamate and sulfate baths the stress values increased from 45.9 to 74.8 MPa and form 106 to 144.8 MPa respectively. Optical micrograph was used for observing cross section of the coatings and it revealed that the deposits have laminar structure. TEM was used to determine microstructure of the coatings and it was found that the microstructure has dislocation cell structure and their grains were surrounded heavily by dense dislocations. After heat treatment, one find the Ni_3P precipitates mainly at grain boundaries of the deposit. The shape of the Ni_3P precipices transforms from round to needle like when heat treated from 343 to 490°C. Thermal analysis was done and it showed two exothermic peaks one of which is for Ni_3P precipitates and the other one is for recrystallization at 575°C.

D.H. Jeong et al [61] studied the hardness and its relation with wear resistance of the Ni-P nanocrystalline deposits. For this purpose they have used low carbon mild steel (AISI 1010) as a substrate with bath temperature of 70°C and pH 1.5. XRD results showed the line broadening of the diffraction pattern which indicates the reduction in the grain size of the coatings with rise in phosphorous content. The average grain size was close to 1nm when measured with XRD. The hardness of the coatings were related with the phosphorous content and it was revealed that the relation of Taber wear index TWI to the hardness always remains inversely proportional to each other. They observed that in nano-crystalline Ni-P coatings there exists a linear relationship between hardness and abrasive wear resistance. Heat treatment increases hardness of the coatings due to the precipitation of Ni_3P and hence it causes the decrease in the TWI.

Tsutomu Morikawa et al [62] used nickel citrate electrolyte for the depositing of Ni-P alloy coatings via electrodeposition method. They used copper sheet as a substrate and the effects of H_2PHO_3 concentration, bath pH, current density and temperature were studied. It was revealed that the current efficiency reaches to a maximum value with the 0.2M concentration of H_2PHO_3. When the current density increases up to $10A/dm^2$, the current efficiencies for both nickel and phosphorous decreases. Increase bath

temperatures increases the current efficiencies for both Ni and P in the deposition of Ni-P in the same proportion and same trend was seen when the pH of the bath was increased. This behavior shows a strong interaction that exists between Ni and Ni-P during Ni-P alloy deposition. Hence it can be said that the alloy formed through direct deposition mechanism. The formation of Ni_3P, Ni_2P and PH_3 was observed at low bath pH.

Chapter 3

Experimentation Methods

This chapter elaborates substrate and sample preparation and enlightens the work methodology used throughout the research work. Also it includes a small introduction of characterization techniques used to characterize samples.

3.1 Substrate Preparation

Required size of substrates were obtained by cutting the HSLA sheet into a square having the dimensions of (25 x 25 x 2) mm^3 via sharing machine. After cutting of the substrate they were grounded roughly in order to remove burn and edges which were left after the machining process. Then one side of all the samples was selected for the coating and was further grounded with different emery (SiC) paper having different grit sizes of 320, 400, 600, 800, 1000, 1200, 1500 and 2000 respectively. The final surface finish obtained was smooth, free of corrosion product, oxide layers, oil and grease. For polishing the surfaces, alumina paste was used in order to obtain mirror like surface. After polishing, the substrates were cleaned with soap water consisting of 30 g/L sodium phosphate carbonate, 30 g/L sodium, and 50 g/L sodium hydroxide for 5 minutes at 80°C. Then they were washed in hot water in order to remove soap and dirt particles and dried under the hot air. Last step was to sonicate them in ethanol bath for 30 minutes for degreasing purpose.

3.2 Preparation of Deposition Bath

The electrodeposition bath was prepared by using $NiSO_4.6H_2O$ (nickel sulphate hexahydrate), $Na_2WO_4.2H_2O$ (sodium tungstate dihydrate), $NaH_2PO_2.H_2O$ (sodium hypophosphite), H_3BO_3 (boric acid), $Na_3C_6H_5O_7.2H_2O$ (sodium citrate) and for fabricating four different types of composite coatings, amount of 0.1g/L, 0.2g/L 0.4g/L and 0.8g/L alumina (Al_2O_3) nanoparticles were added in separate beakers.

3.3 Sample Preparation

Specific amount of each chemical was mixed in deionized water in order to prepare electrolyte solution for electrodeposition process. All the chemicals taken were of high purity and sourced form Sigma Aldrich, Darmstadt, Germany. For the composite coatings, required amount of alumina nanoparticles needed to incorporate in Ni-W-P matrix were added in electrolyte bath prior to electrodeposition. The electrolyte was then probe sonicated for 45 minutes and its temperature was risen by using hotplate. Prior to electrodeposition coating; each sample substrate was etched with 20% HCl for 20 seconds in order to trigger the surface and then washed in distilled water and was immediately dipped in the electrolyte for the coating to be deposited in the presence of the applied external AC current. The continuous agitation was also done with the magnetic stirrer at 300 rpm throughout the electrodeposition process to avoid any settling or agglomeration of particles present in the electrolyte bath. Half hour was given to the electrodeposition process and after that the sample was taken off from the electrolytic bath, washed with lukewarm water, dried and covered with butter paper and placed in a desiccator. The schematic diagram of substrate and sample preparation is shown in Figure 3.1. Composition of the electrolyte and optimized bath operating parameters are presented in **Table 3.1** and **Table 3.2** respectively. The composition of HSLA steel substrate is given in **Table 3.3**.

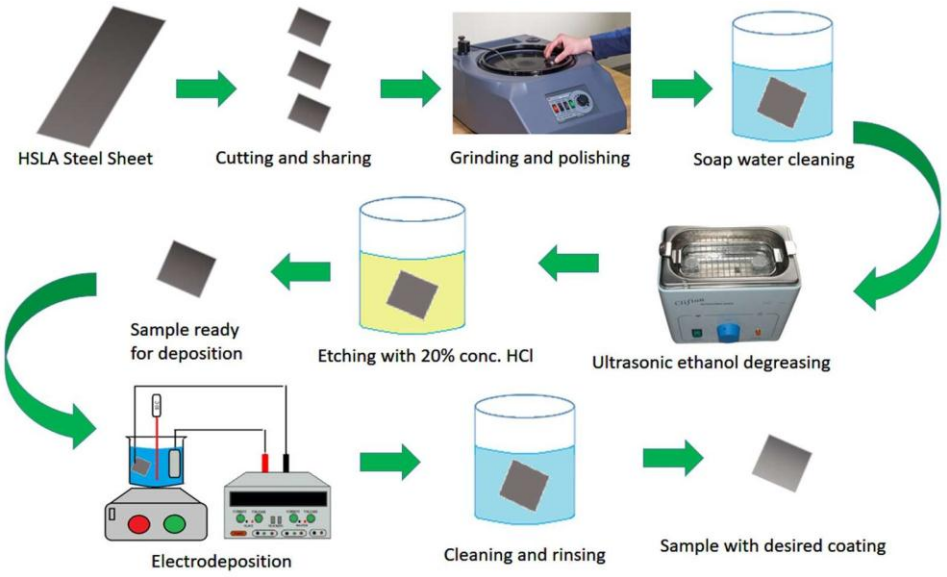

Figure 3.1. A schematic diagram of substrate and sample preparation.

Table 3.1. Composition of Ni-W-P/Al2O3 electroplating bath.

Chemicals	Nickel Sulphate Hexahydrate	Sodium Tungstate dihydrate	Sodium Hypophosphite	Boric Acid	Sodium Citrate	Alumina Particles
Amount g/L	25	80	12	40	80	0.1, 0.2, 0.4 and 0.8

Table 3.2. Optimized electroplating bath parameters.

Temperature	**pH**	**Current**	**Etching Time in 20% HCl**	**Coating Time**
80°C	~9	0.1A	20 seconds	30 minutes

Table 3.3. Elemental composition of high strength low alloy (HSLA) steel substrate.

Elements	C	Si	Mn	Ni	Cr	P & S	Fe
wt.%	0.27~0.29	1.2~1.4	0.8~1.0	0.3	1.0~1.2	0.025	Balance

3.4 Analysis and Characterizations of as Deposited Ni-W-P Alloy and Ni-W-P/Al_2O_3 Composite Coatings:

3.4.1 SEM and EDX Analysis

The surface morphologies and chemical composition of Ni-W-P (Al_2O_3) composite coatings were analyzed by using JEOL JSM-6490A analytical scanning electron microscope (SEM) from Japan equipped with energy dispersive spectroscopy (EDX) analyzer. SEM was used to analyze surface morphologies whereas EDX technique is used for composition analysis. Further, the architecture of coatings developed after wear testing was also examined using SEM study.

3.4.2 AFM Analysis

The topography of the composite coatings was performed using JEOL JSPM-5200 atomic force microscopy (AFM) from Japan through which the thickness and roughness of the coatings were studies. AFM analysis allows to investigate topographical features and surface properties of deposited coating surfaces with nanometer resolution.

3.4.3 Nanoindentation (Hardness and Elastic Modulus)

For mechanical properties like hardness and young's modulus, nanoindentor; iMirco (nano-mechanics) USA, attached to AFM was utilized using berkovich indenter tip to measure nanoindentation values. The obtained results consisted of the average of five readings. Nano-indentation testing was performed at a maximum load and strain rate of 5mN force and 0.2 s^{-1} respectively. The data was drawn in the form of load verses displacement (nm) curves by employing Oliver-Pharr method which is used to analyze mechanical properties of coatings such as hardness, elastic modulus and hence the stiffness etc.

3.4.4 Wear Analysis

The wear behavior of as-deposited coatings was investigated using ball on disk tribometer (MT/60/NI) from Spain. The sliding velocity was retained persistent at a rate of $0.11ms^{-1}$ having the diameter of 5mm. The interacting ball was made of stainless steel and the deposited surface coatings acted as a disk. The experiment was done under room temperature with 1N load and a sliding distance of 110m.

3.4.5 Electrochemical Analysis

For electrochemical analysis potentiodynamic polarization (PP) method was utilized. All the electrochemical tests were performed in a brine solution containing 3.5 wt% NaCl. For PP test the GAMRY potentiostat interface 1010E was used to determine corrosion behavior of Ni-W-P alloy and Ni-W-P/Al_2O_3 composite coatings. The electrochemical cell was consisted of three electrode system in which the graphite electrode was used as a counter electrode, Ag/AgCl was taken as a reference electrode, whereas the coated sample was taken as a working electrode. The tests were performed with a scanning rate of 1mV/s and potential window from -1.5 to 0.5 mV to acquire anodic and cathodic polarization curves.

Chapter 4

Results and Discussions

4.1 SEM Analysis

The SEM images in **Figure 4.1** reveal dense and uniform coatings electrochemically deposited on HSLA steel substrate successfully. It can be seen that all coatings possess regular nodular morphology for both figure 5 and 6. A spherical nodular morphology helps enhance the wear resistance of coatings as it is self-lubricating in nature which finally results in lower FC. A nodular morphology of alloys based on nickel coatings have been stated by many researchers [63] [64]. Such structures act as lubricant pockets [65]. This lubrication effect is more prominent for the Ni-W-P/BN composite coatings as two dimensional embedded BN sheets provide lubrication. The grain size of the coating can be seen to decrease by adding nano alumina particles. This is primarily due to the fact that alumina particles, once embedded, inhibit lateral grain growth of the Ni grains. There is a significant difference of grain size between pure Ni-P-W coatings and the ones that are reinforced with nano-alumina particles. A morphology of the coatings is seen to get finer as the concentration of reinforcement increased. This change in morphology and grain size has a noteworthy effect on the roughness, mechanical and corrosion resistant properties of the composite coatings, as seen in the later sections. When the concentration of alumina increases to 0.4g/L and beyond, small pores or voids can be seen to exist on the surface of the coatings. These pores generate due to the agglomeration of alumina nano particles in the Ni-P-W matrix, preventing adequate deposition of the matrix between them. **Figure 4.3** presents a cross-sectional view of the coatings, revealing their average thickness and variations in it. The average thickness of the coating(s) measured is around 44.337µm, with little deviations. Furthermore, due to the electrodeposition process, the coatings can be seen to be firmly attached on the surface of HSLA substrates with little to no voids in the interface.

SEM images of Ni-W-P/BN composite coatings **Figure 4.2** reveal that by adding different amounts of BN, each coating maintained its nodular morphology whereas when the concentration of BN increases, the number of nodules increases. No pores

and cracks are seen in each coating. Till BN concentration of 0.2g/L, the structure seems to be homogeneous, whereas above 0.2g/L BN some agglomeration took place because of greater amount of BN in the electrolyte. Also, the structure seems to get refined with greater amount of BN which has a direct effect on mechanical and corrosion resistant properties.

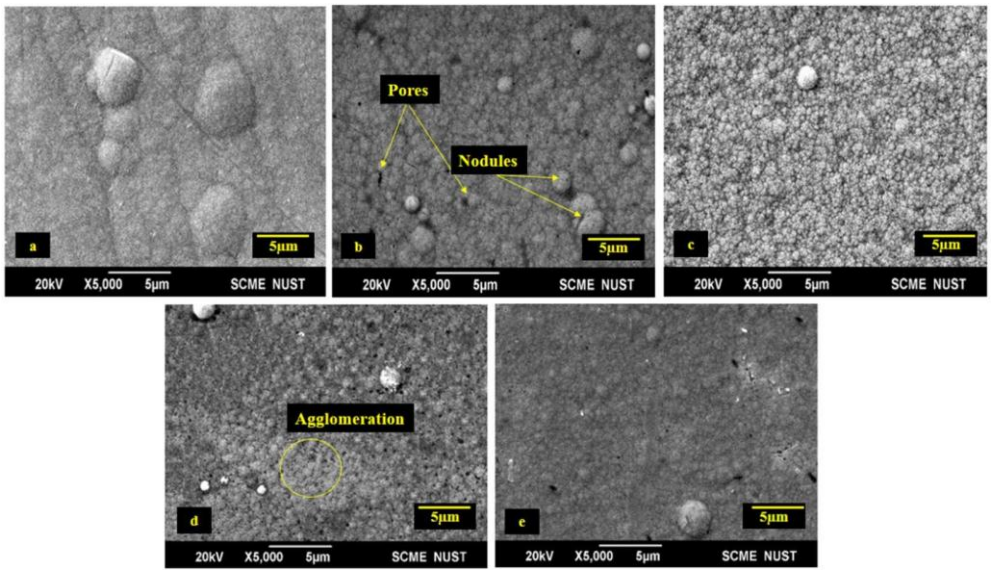

Figure 4.1. SEM images of (a) Ni-W-P alloy coating, (b) Ni-W-P composite coating with 0.1g/L Al2O3 (c) 0.2g/L Al2O3 (d) 0.4g/L Al2O3 and (e) 0.8g/L Al2O3.

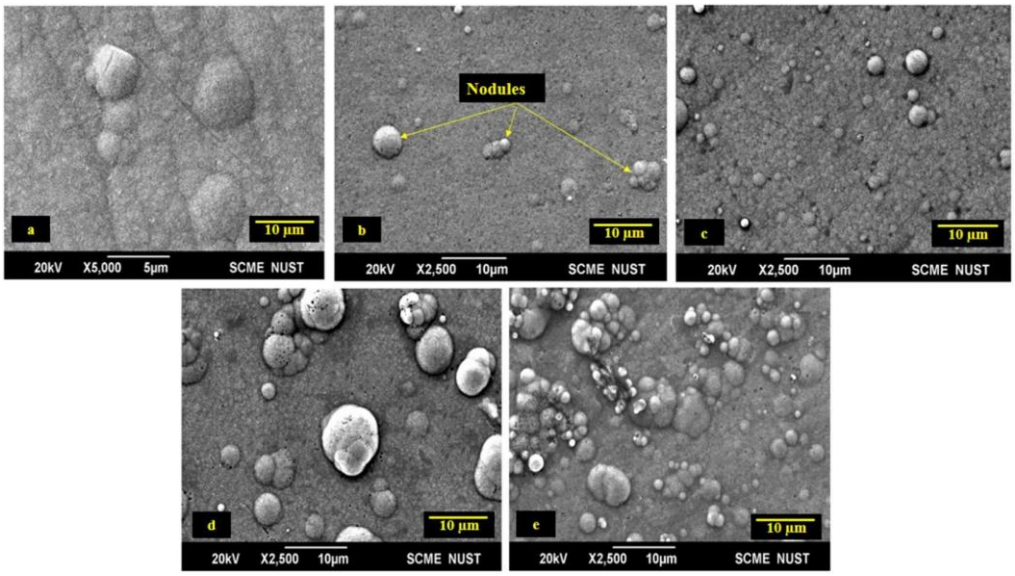

Figure 4.2. SEM images of (a) Ni-W-P alloy coating, (b) Ni-W-P composite coating with BN (0.1g/L) (c) BN (0.2g/L) (d) BN (0.4g/L) and (e) BN (0.8g/L)

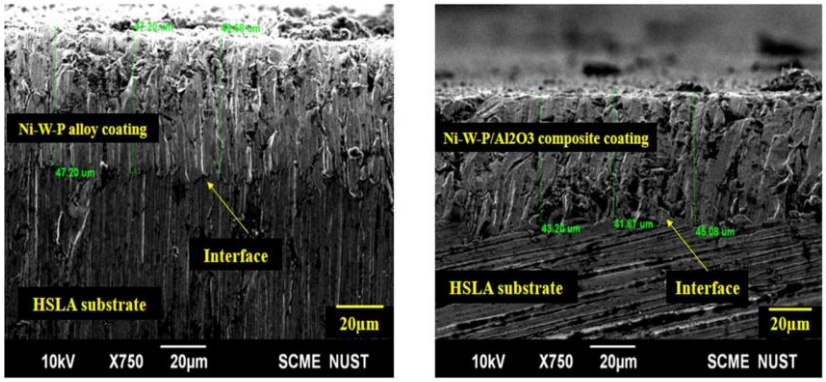

Figure 4.3. Cross sectional view of Ni-W-P alloy and Ni-W-P/ Al2O3 composite coatings revealing the lamellar structure.

4.2 EDS Analysis

EDX analysis confirmed the deposition of Ni, W, P and Al_2O_3 particles which were used for the fabrication of coatings and are represented by their respective elemental

peaks. Their relative amounts in wt% are displayed in **Table 4.1**. It can be seen that the deposits consists of low phosphorous content i.e. < 7%. Ni coatings consisting of low phosphorous content exhibits a nano crystalline structure as reported by many researchers[66, 67]. This crystallinity has the significant effect on the mechanical and corrosion resistant properties of the composite coatings. EDX elemental mapping of 0.2g/L alumina nanoparticles demonstrates a even distribution of all the elements in the Ni-W-P/Al_2O_3 coating. An increase in the Al wt% can be observed as the concentration of nano alumina increases.

EDX analysis for Ni-W-P/BN composite coatings shows that the required elements has been deposited in each coating except the coating with 0.1g/L BN. This is because of the limitation of SEM equipment, very less amount of BN in the electrolyte and smaller atomic size of boron element. From the EDX data, one can discern that as the BN concentration increases in the electrolyte, the phosphorous content decreases significantly when compared to tungsten content. This shows that BN is deposited in expense of phosphorous content. It can also be seen that with increase of BN amount in the electrolyte, the concentration of BN in as-deposited coatings also increases. The values can be seen from the **Table 4.2**.

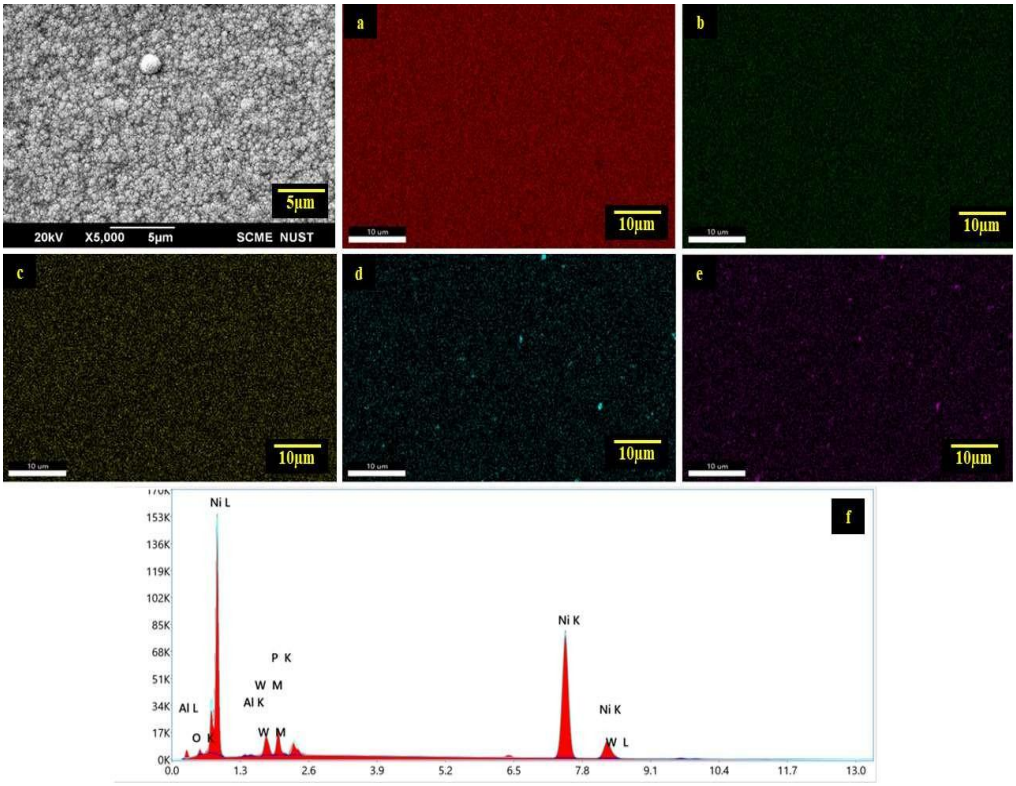

Figure 4.4. Elemental mapping of Composite Coating (a) Nickel (b) Phosphorous (c) Tungsten (d) Aluminum (e) Oxygen and (f) EDX study of Ni-W-P/ Al_2O_3 (0.2g/L) composite coating.

Table 4.1. EDX analysis of Ni-W-P alloy and Ni-W-P/ Al_2O_3 composite coating.

Chemical Composition (wt%)					
Sample Name	**Nickel**	**Phosphorous**	**Tungsten**	**Aluminum**	**Oxygen**
Ni-W-P	83.8	5.8	10.4	-	-
Ni-W-P/Al_2O_3 (0.1g/L)	83.4	4.3	11.4	0.2	0.7
Ni-W-P/Al_2O_3 (0.2g/L)	82.9	4.2	11.2	0.5	1.2
Ni-W-P/Al_2O_3 (0.4g/L)	82.1	4.2	11.7	0.6	1.4
Ni-W-P/Al_2O_3 (0.8g/L)	82.7	4.0	11.5	0.7	1.1

Table 4.2. EDX analysis of Ni-W-P alloy and Ni-W-P/BN composite coating.

Chemical Composition (wt%)					
Sample Name	**Nickel**	**Phosphorous**	**Tungsten**	**Aluminum**	**Oxygen**
Ni-W-P	83.8	5.8	10.4	-	-
Ni-W-P/BN (0.1g/L)	83.6	3.6	11.7	-	1.1
Ni-W-P/ BN (0.2g/L)	83.2	3.2	11.3	0.3	2.0
Ni-W-P/ BN (0.4g/L)	82.1	2.6	10.5	0.7	4.1
Ni-W-P/ BN (0.8g/L)	81.4	2.5	8.8	1.4	5.9

4.3 Atomic Force Microscopic (AFM) Analysis

The apparent roughness of the coatings were analyzed via AFM technique. AFM images also confirms a nodular morphology and as concentration of alumina particles increases beyond 0.2g/L, it results in an agglomeration of reinforcement. This agglomeration results in an increase in the roughness of the coating as shown in **Figure 4.5** which is in consistent with the previously reported data [67]. Surface morphology and roughness tend to have a noteworthy influence on the hardness and wear performance of the coatings. Roughness values of HSLA steel, Ni-P-W alloy and composite coatings are listed in **Table 4.3**.

AFM results for Ni-W-P/BN composite coatings **Figure 4.6** showed that with the increase amount of BN, the roughness of coatings keep increasing and it can be attributed to the formation of small agglomerates which leads to high roughness. This can be cross-checked with the SEM images of the coatings. The roughness values are given in the **Table 4.4**. When compared the results of Ni-W-P/BN with Ni-W-P/Al_2O_3, for BN the roughness increases significantly while for Al_2O_3, the roughness although increases but with lesser amount. This can be associated with the dangling bonds of 2D exfoliated BN sheets as they can easily bond together in electrolyte or while deposition because of the high surface energy, hence increasing the roughness of the coatings. Also when the concentration of particles after a certain loading increases in the electrolyte, agglomeration takes place because the mean distance between them decreases.

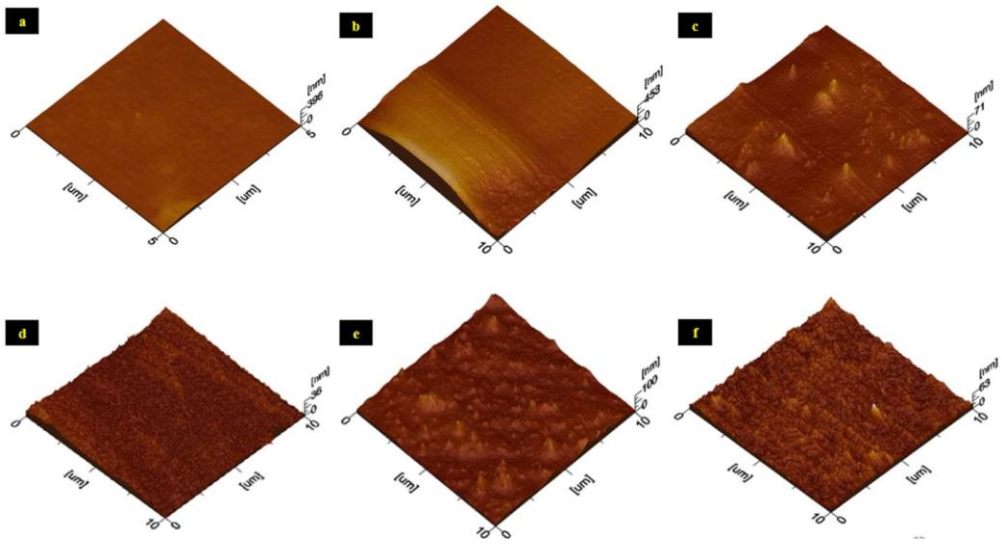

Figure 4.5. AFM images of (a) HSLA Steel (b) Ni-W-P alloy (c) Ni-W-P/Al_2O_3 (0.1g/L) (d) Ni-W-P/Al_2O_3 (0.2g/L) (e) Ni-W-P/Al_2O_3 (0.4g/L) and (f) Ni-W-P/Al_2O_3 (0.8g/L)

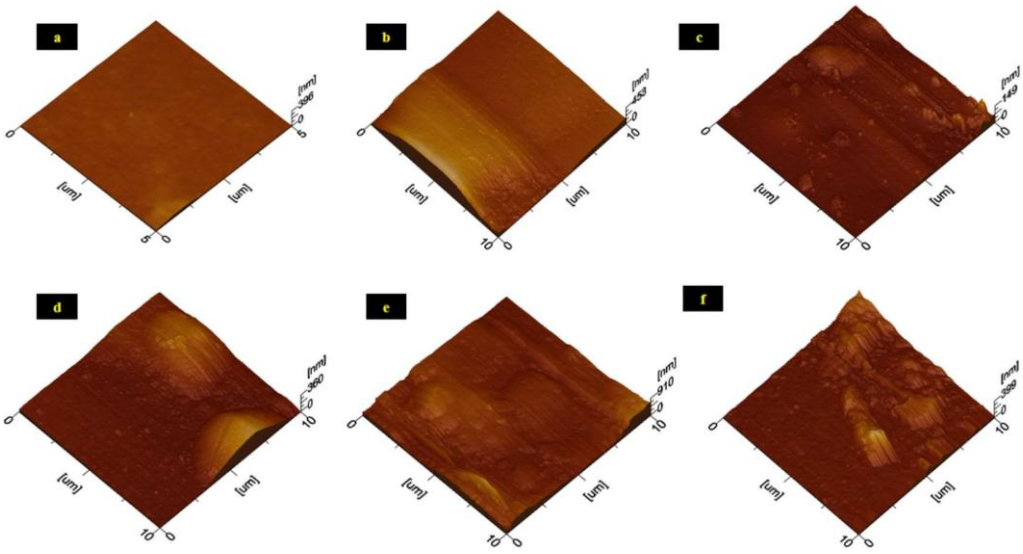

Figure 4.6. AFM images of (a) HSLA Steel (b) Ni-W-P alloy (c) Ni-W-P/BN (0.1g/L) (d) Ni-W-P/ BN (0.2g/L) (e) Ni-W-P/ BN (0.4g/L) and (f) Ni-W-P/ BN (0.8g/L)

Table 4.3. Roughness values of HSLA steel, Ni-W-P alloy and Ni-W-P/ Al_2O_3 composite coatings.

Sample Name	**Roughness Ra (nm)**
HSLA Steel	4.59
Ni-W-P	4.70
Ni-W-P/Al_2O_3 (0.1 g/L)	5.86
Ni-W-P/Al_2O_3 (0.2 g/L)	6.22
Ni-W-P/Al_2O_3 (0.4 g/L)	8.40
Ni-W-P/Al_2O_3 (0.8 g/L)	8.93

Table 4.4. Roughness values of HSLA steel, Ni-W-P alloy and Ni-W-P/BN composite coatings.

Sample Name	**Roughness Ra (nm)**
HSLA Steel	4.59
Ni-W-P	4.70
Ni-W-P/BN (0.1 g/L)	9.35
Ni-W-P/ BN (0.2 g/L)	40.5
Ni-W-P/ BN (0.4 g/L)	64.1
Ni-W-P/ BN (0.8 g/L)	82.4

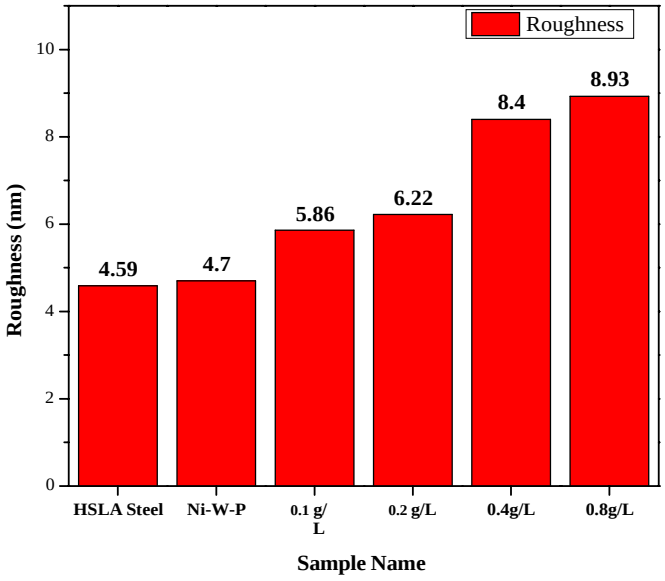

Figure 4.7. Roughness values of HSLA, Ni-W-P alloy and Ni-W-P/Al_2O_3 composite coatings with different alumina concentrations are presented. The graph shows that roughness values increases as we increase concentration of alumina particles.

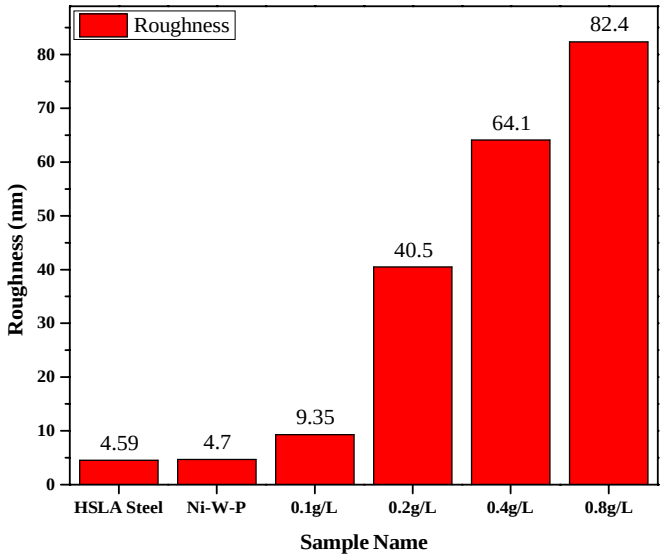

Figure 4.8. Roughness values of HSLA, Ni-W-P alloy and Ni-W-P/BN composite coatings with different boron nitride concentrations are presented.

4.4 Nano-Indentation

Nano-indentation tests were performed to grasp the better understanding of mechanical properties like hardness (a property of a material that enables it to resist penetration, scratching, abrasion or cutting) and elastic modulus of the coatings. Where it revealed that with the increment of alumina particles, the hardness of the coatings increases to the significant amount and with further increment of alumina particles it decreases [68] as shown in the **Figure 4.9**.

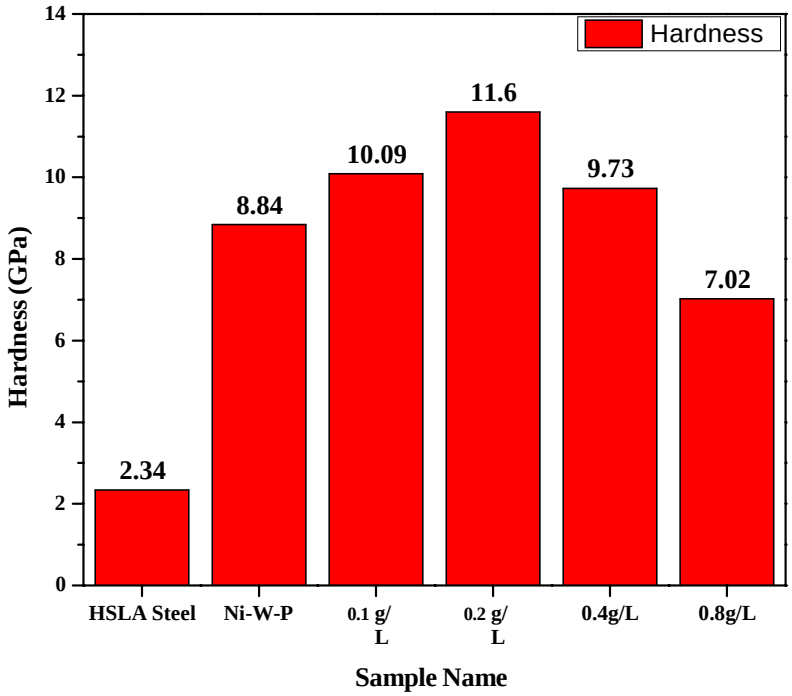

Figure 4.9. Comparison of hardness values of HSLA, Ni-W-P alloy and Ni-W-P/ Al_2O_3 composite coatings with different alumina concentrations are presented. The trend shows that hardness of coatings increases till 0.2g/L alumina concentration followed by decrease in hardness.

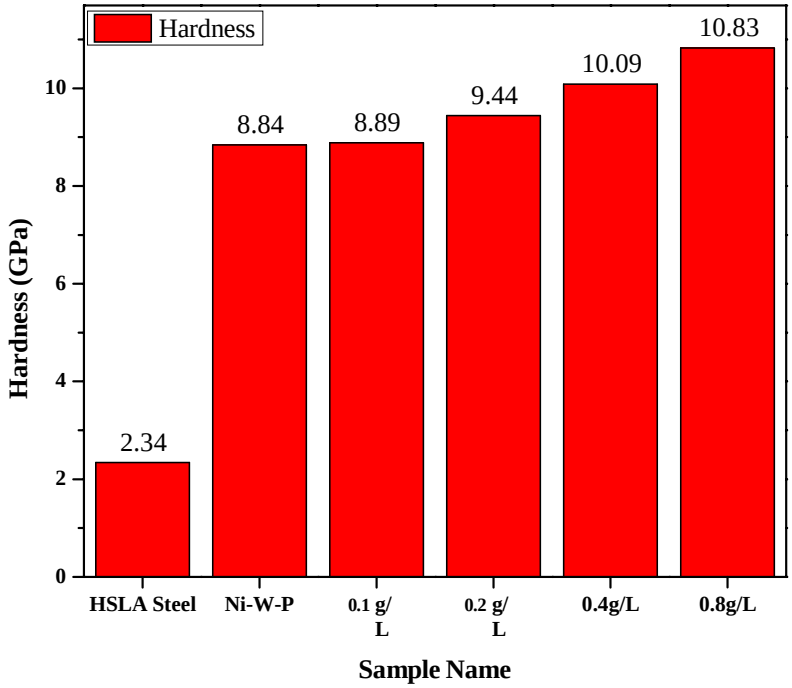

Figure 4.10. Comparison of hardness values of HSLA, Ni-W-P alloy and Ni-W-P/BN composite coatings with different BN concentrations are presented. The trend shows that hardness of coatings increases for each loading.

The best hardness and elastic modulus values for the coating alumina 0.2g/L came out to be 11.60 GPa and 194.18 GPa respectively. This increase in hardness can be attributed to the uniform distribution of alumina particles (dispersion hardening) which decreases the crystal size of the matrix (Ni) resulting the increase in the microhardness of the coating by reinforcing the grain boundaries. As mentioned earlier that the alumina inclusion altered the surface conditions, both the grain boundaries and the dislocation density are increased and hence supported the formation of finer grains which results in high hardness. When the load-depth graphs of the Ni-W-P composite coatings shown in the **Figure 4.11** were examined, it is observed that the indentation depth drastically decreased from HSLA steel substrate to Ni-W-P alloy coating and is further decreased till 0.2g/L alumina loading. This confirms that the hardest coating is obtained with 0.2g/L

alumina particles indicating that the material's microstructure is fine, compact and homogeneous. The nano-indentation depth increases when the microstructure of the material is coarse and heterogeneous [69]. Similarly, the elastic modulus can also be obtained from load-depth profiles and with the decrease in indentation depth, the elastic modulus increases. The area under the curve also decreases till the amount of 0.2g/L alumina revealing that the coatings are hard. With further increase of alumina particles, the area under the curve (loading and unloading curve) increases hence the hardness decreases and this can be attributed to the agglomeration and inhomogeneous distribution of particles that can be seen in SEM images. The values of hardness, Elastic modulus and their ratios are given in the **Table 4.5**. The hardness of the coatings increased due to (i) the formation of dense and compact structure, (ii) embedded hard ceramic nanoparticles of Al_2O_3, (iii) solid state hardening due to the co-deposition of W and dispersion hardening as a result of uniform dispersion of alumina particles in the Ni-W-P/Al_2O_3 composite coating, (iv) generation of refined structure [68].

As hardness depends upon the nature of embedded particles, hardness of Ni-W-P/BN composite coatings also increases when compared with Ni-W-P alloy due to the refinement of the nickel matrix but is less than the nano-alumina inclusion. In case of BN addition, the hardness increases for each loading as can be seen from the **Figure 4.10** and **4.12**. The values of hardness and elastic modulus for BN are given in **Table 4.6**.

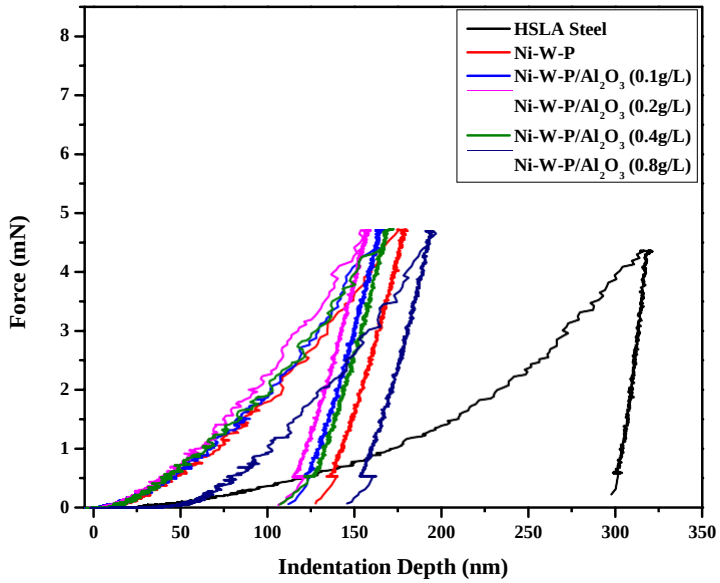

Figure 4.11. Loading and unloading curves between force and indentation depth for HSLA steel, Ni-W-P alloy and Ni-W-P/ Al_2O_3 composite coatings.

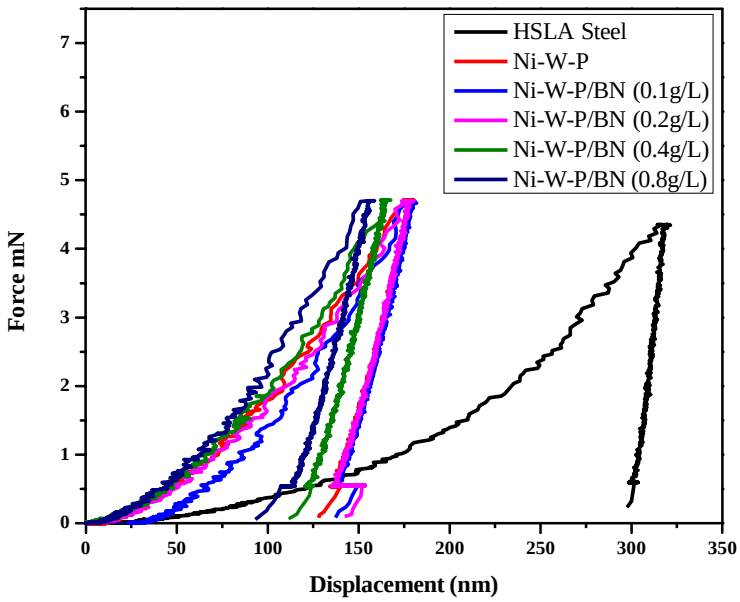

Figure 4.12. Loading and unloading curves between force and indentation depth for HSLA steel, Ni-W-P alloy and Ni-W-P/BN composite coatings.

Table 4.5. Nano-indentation values for HSLA steel, Ni-W-P alloy and Ni-W-P/Al_2O_3 composite coatings

Sample Name	**Hardness GPa**	**Elastic Modulus GPa**	**H/E Ratio**
HSLA Steel	2.34	225.55	0.0104
Ni-W-P	8.84	161.27	0.0548
Ni-W-P/Al_2O_3 (0.1 g/L)	10.09	178.69	0.0564
Ni-W-P/ Al_2O_3 (0.2 g/L)	11.60	194.18	0.0597
Ni-W-P/ Al_2O_3 (0.4 g/L)	9.73	170.34	0.0571
Ni-W-P/ Al_2O_3 (0.8 g/L)	7.02	157.76	0.0445

Table 4.6. Nano-indentation values for HSLA steel, Ni-W-P alloy and Ni-W-P/BN composite coatings

Sample Name	**Hardness GPa**	**Elastic Modulus GPa**	**H/E Ratio**
HSLA Steel	2.34	225.55	0.0104
Ni-W-P	8.84	161.27	0.0548
Ni-W-P/BN (0.1 g/L)	8.89	168.93	0.0526
Ni-W-P/BN (0.2 g/L)	9.44	184.35	0.0512
Ni-W-P/BN (0.4 g/L)	10.09	187.69	0.0537
Ni-W-P/BN (0.8 g/L)	10.83	190.45	0.0569

4.5 Wear Tribology

Wear tribology graphs obtained for the alloy and Ni-W-P/Al_2O_3 composite coatings are presented in **Figure 4.13**. The texture of the surface is measured by surface roughness which plays an important role when the surfaces are in contact. It can be perceived that the friction co-efficient of the coatings lies between 0.22 and 0.65 which tells us that the coatings are dry. As seen in **Figure 4.13** the FC of HSLA steel and Ni-W-P is unstable with large fluctuations for almost the whole distance and this can be attributed to the severe adhesion wear that occurred during the period of

sliding[67]. The wear coefficient of the alloy and the composite coatings for the alumina amount till 0.2g/L decreases to the value of 0.2255 and then it increases to the value of 0.5537 for the alumina amount 0.4 and 0.8g/L as seen from the **Table 4.7** and their comparisons can be drawn from the **Figure 4.15.**

The surge in the friction co-efficient can be ascribed to the presence of hard alumina particles which while tribology testing; helped reinforcing the wear mechanism. Also as the roughness of the composite coatings is increasing, shear forces also increasing which leads to high values of FC in nanocomposite coatings. (ii) One can observe from the graphs that there is a high wear loss in initial running in-period for the coatings and then they attain steady state wear. After distance of 40m, steady state wear occurs and values were measured after this distance.

Wear tribology graphs for Ni-W-P/BN composite coatings are presented in **Figure 4.14**. Through these graphs it is shown that the friction co-efficient for each loading of BN decreases. The values of FC are presented in **Table 4.8** and shown in the **Figure 16**. FC values decreases significantly when compared with alloy and Ni-W-P/BN (0.8g/L) from 0.4231 to 0.0710 respectively. This decrease in FC value shows the lubricant behavior of boron nitrite particles.

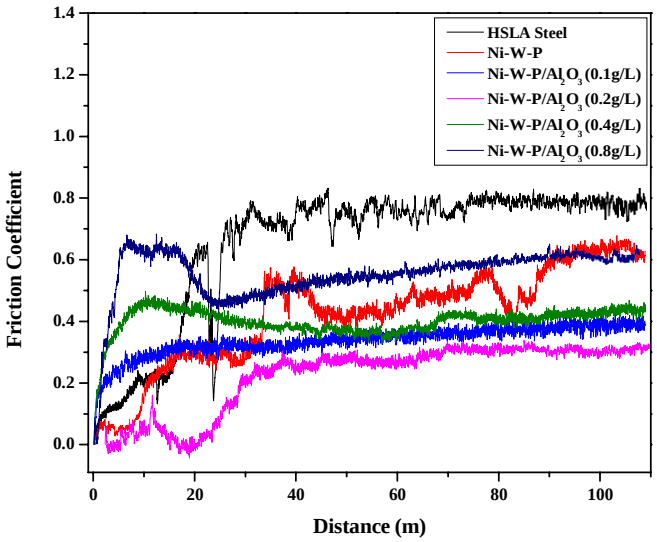

Figure 4.13. Wear tribology graph of HSLA Steel, Ni-W-P alloy and Ni-W-P/Al_2O_3 composite coatings showing the friction-coefficient trend with increasing distance.

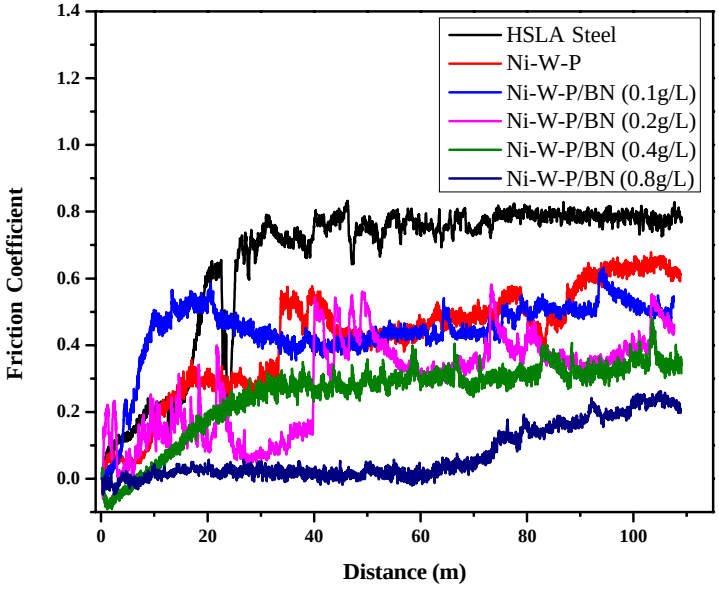

Figure 4.14. Wear tribology graph of HSLA Steel, Ni-W-P alloy and Ni-W-P/BN composite coatings showing the friction-coefficient trend with increasing distance.

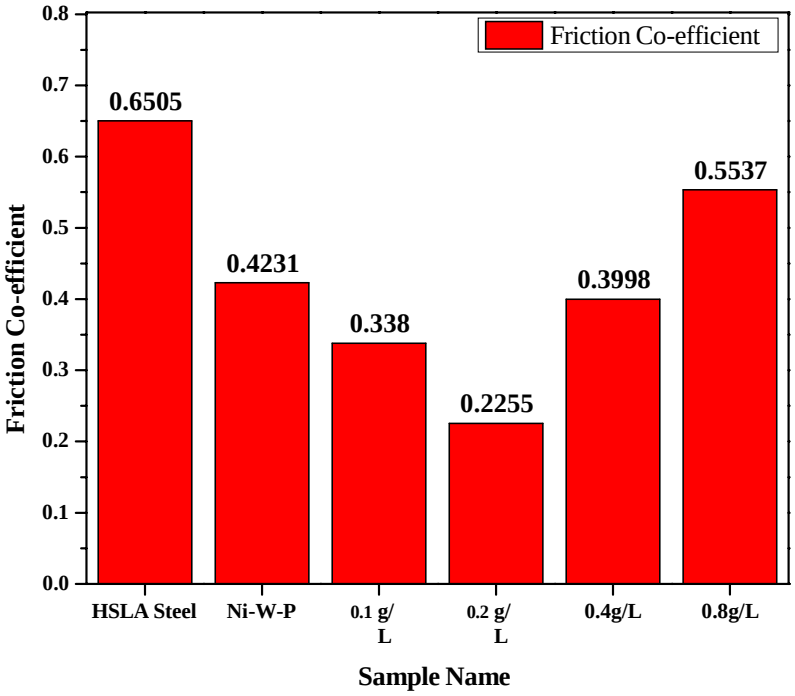

Figure 4.15. Comparison of friction coefficient values of HSLA steel substrate, Ni-W-P alloy and Ni-W-P/Al_2O_3 composite coatings with different alumina concentrations. The trend shows first decrease in FC till 0.2g/L alumina inclusions followed by increase in FC values.

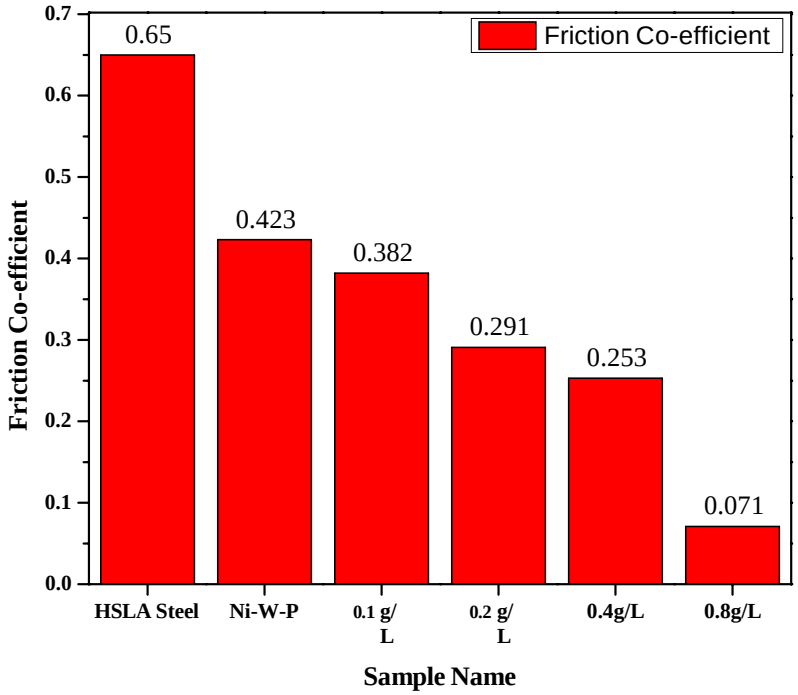

Figure 4.16. Comparison of friction coefficient values of HSLA steel substrate, Ni-W-P alloy and Ni-W-P/BN composite coatings with different boron nitrite concentrations. The trend shows that FC of coatings decreases for each loading.

Table 4.7. Wear tribology values (friction co-efficient and wear rate) of as deposited coatings.

Sample Name	**Friction Co-efficient**	**Wear Rate (mm^3/m)**
HSLA Steel	0.6505	6.539×10^{-6}
Ni-W-P	0.4231	1.834×10^{-7}
Ni-W-P/Al_2O_3 (0.1 g/L)	0.3380	9.962×10^{-8}
Ni-W-P/Al_2O_3 (0.2 g/L)	0.2255	1.946×10^{-8}
Ni-W-P/Al_2O_3 (0.4 g/L)	0.3998	3.111×10^{-8}
Ni-W-P/Al_2O_3 (0.8 g/L)	0.5537	7.954×10^{-7}

Table 4.8. Wear tribology values (friction co-efficient and wear rate) of as deposited coatings.

Sample Name	Friction Co-efficient	Wear Rate (mm^3/m)
HSLA Steel	0.6505	6.539×10^{-6}
Ni-W-P	0.4231	1.834×10^{-7}
Ni-W-P/BN (0.1 g/L)	0.3823	2.692×10^{-8}
Ni-W-P/ BN (0.2 g/L)	0.2910	2.439×10^{-8}
Ni-W-P/ BN (0.4 g/L)	0.2528	2.231×10^{-8}
Ni-W-P/ BN (0.8 g/L)	0.0710	6.634×10^{-10}

SEM images of wear tracks for Ni-W-P/$Al_2O_3$are also presented in the **Figure 4.17**. When the load is applied during tribological testing, plastic deformation and the combination of stresses like tensile, compression, shear and brittleness of the material occur due to which the as-electrodeposited coatings get cracked rapidly and simply detach from the metal surface (substrate). This led to the initiation of cracks from the sub-surface causing delamination of as-deposited coatings. A remarkable surface damage, micro-cracks, wear debris and the material removal in patches can be seen from SEM images of HSLA steel and Ni-W-P alloy coating **Figure 4.17**(a & b) respectively. This can be attributed to the delamination, micro-ploughing and fracture that occurred between the two surfaces representing the adhesive nature of wear mechanism. Further with the addition of 0.1g/L alumina particles **Figure 4.17c**, although the globular morphology has been entirely deformed; it still shows plastic deformation and fatigue cracks along with micro-ploughing on the worn out surface which generated by cyclic loading and surface deformation. But when 0.2g/L alumina particles were added which is shown in the **Figure 4.17d,** the plastic deformation is decreased to some extend and the coating somewhat preserved its globular morphology and some micro-cracks were seen on the worn scar. This can be due to the decrease in plasticity of Ni-P-W and increase in hardness value i.e. 11.60 GPa due to the addition of Al_2O_3 nanoparticles that helped in developing a greasy layer on the worn scar, hence, showing low friction of co-efficient and wear rate. The best coating was obtained with 0.2g/L alumina particles having the friction coefficient of 0.2255

and the minimum wear rate of 1.946× 10^{-8}. The parallel scratches/ fine grooves appeared along the sliding direction as shown in **Figure 4.17e** and some pits are formed which indicates abrasive wear mechanism because of the synergic effect of both micro ploughing and micro-cutting of hard counterface. This indicates that the tribological behavior of Ni-W-P/Al_2O_3 composite coatings is the mixture of adhesive wear and abrasive wear mechanism.

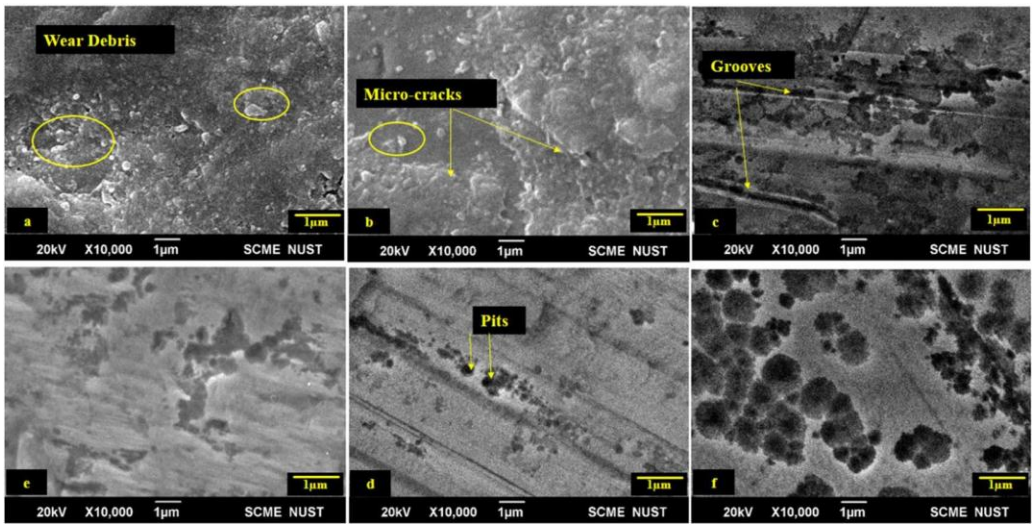

Figure 4.17. SEM images of the wear track (a) HSLA Steel, (b) Ni-W-P alloy, (c) Ni-W-P/ Al_2O_3 (0.1g/L), (d) Ni-W-P/ Al_2O_3 (0.2g/L), (e) Ni-W-P/ Al_2O_3 (0.4g/L) and (f) Ni-W-P/ Al_2O_3 (0.8g/L)

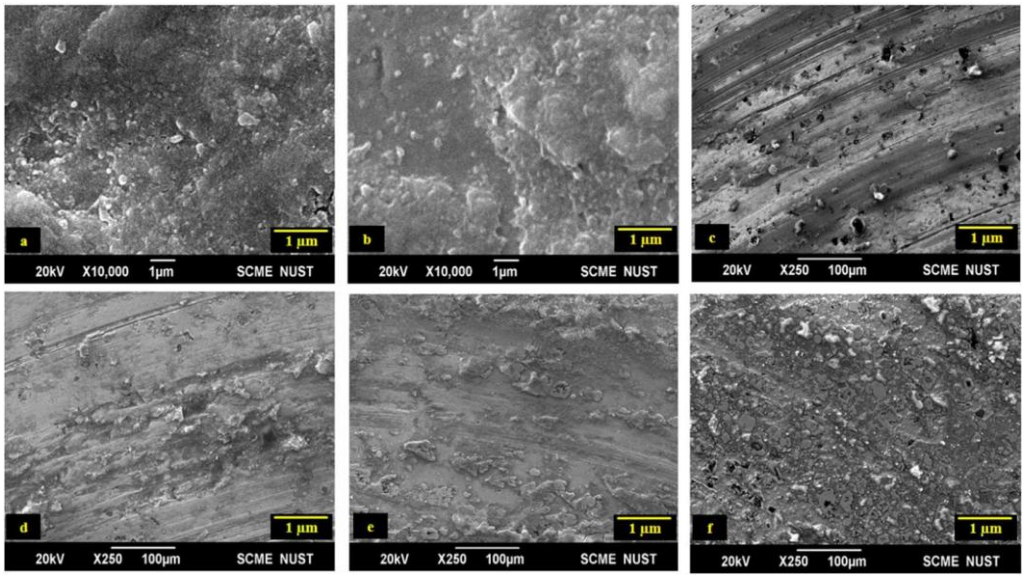

Figure 4.18. SEM images of the wear track (a) HSLA Steel, (b) Ni-W-P alloy, (c) Ni-W-P/BN (0.1g/L), (d) Ni-W-P/ BN (0.2g/L), (e) Ni-W-P/ BN (0.4g/L) and (f) Ni-W-P/ BN (0.8g/L)

SEM images of wear tracks for Ni-W-P/BN are presented in the **Figure 4.18**. For BN (0.1g/L and 0.2g/L), one can see a little formation of grooves and some debris. For image c pit formation is also seen. For the images **e and f** no grooves and pits are seen rather few to many exfoliated 2D BN sheets are seen on the surface when the two surfaces slide each other which helped in reducing friction co-efficient between the two surfaces and acted as lubricant. Lesser effects of surface asperities and significant effect of 2D BN sheets are observed. The values of wear rate and friction coefficient are given in **Table 4.8**.

4.6 Potentiodynamic Polarization Behavior of Electrodeposited Coatings

The corrosion behavior of the coatings were studied by conducting potentiodynamic polarization experiment and plotting Tafel plots by extrapolation method from the data. The Tafel plots can be seen in the **Figure 4.19** and it is observed that the coatings become more corrosion resistant with the increment in the alumina particles till

0.2g/L followed by a slight decrease in corrosion resistant behavior, referring **Table 4.9** and **Figure 4.21**. This can be ascribed to some pores and agglomeration of alumina particles. Corrosion performance of the deposits depends on many factors such as (i) amount of the particles added (volume fraction), how homogeneously they got dispersed and the chemical composition of the nanoparticles. (ii) As Al_2O_3 possesses an anti-corrosive properties, increasing its volume fraction with homogeneous distribution in the coatings will result in superior corrosion properties because they create a strong barrier against Cl^- ions, (iii) Matrix condition also have a great influence on corrosion resistant properties of the composite coatings for instance the crystallite size and the porosity content [68].

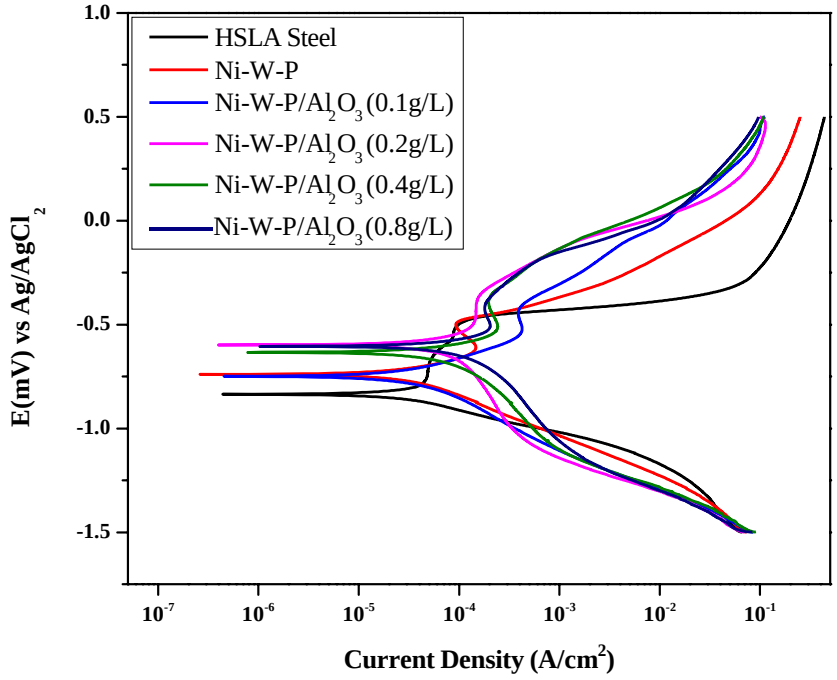

Figure 4.19. Potentiodynamic polarization behavior of HSLA steel, Ni-W-P alloy and composite coatings containing different Alumina (Al_2O_3) concentrations. Tafel plots.

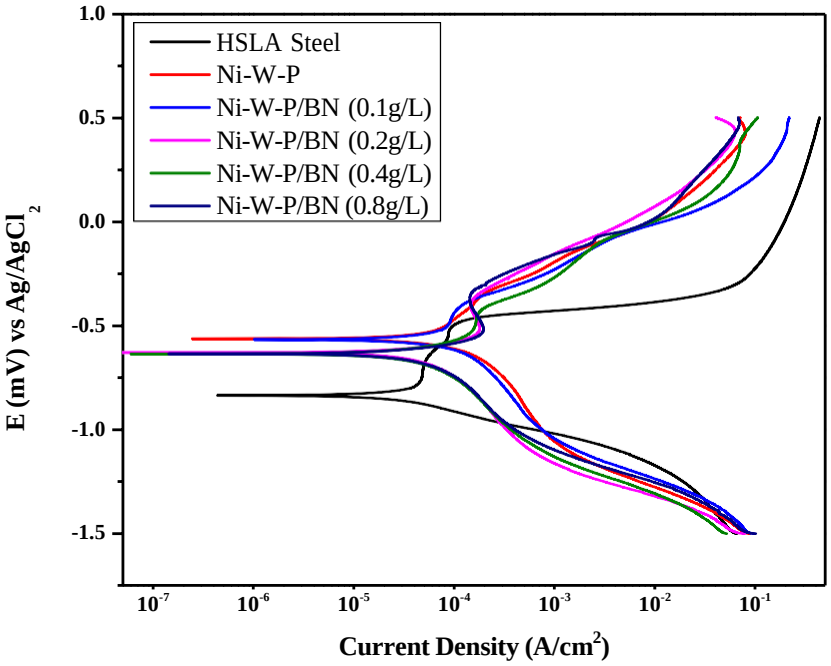

Figure 4.20. Potentiodynamic polarization behavior of HSLA steel, Ni-W-P alloy and composite coatings containing different BN concentrations. Tafel plots.

The Tafel plot for Ni-P-W/BN composite coatings is present in the **Figure 4.20**. The values of i_{corr} obtained through these graphs are presented in **Table 4.10**. It can be seen that with the inclusion of BN particles the CR decreases for each loading. Hence, BN plays a positive role in corrosion resistant properties of the coatings.

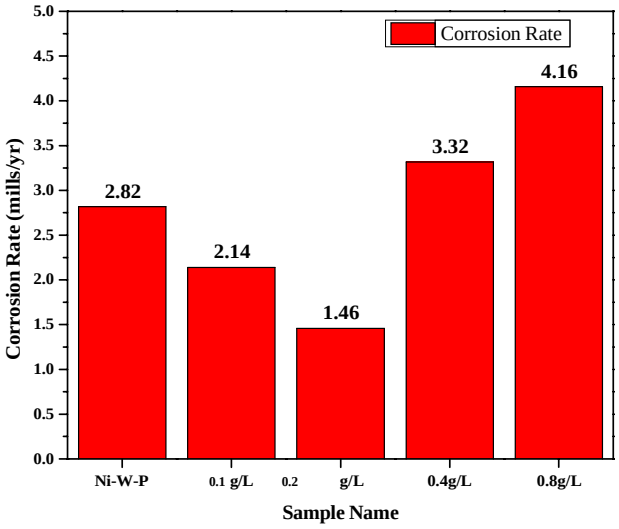

Figure 4.21. Comparison of corrosion rate values of HSLA steel substrate, Ni-W-P alloy and Ni-W-P/ Al_2O_3 composite coatings with different alumina concentrations. Amount 0.2g/L alumina shows the lowest corrosion rate.

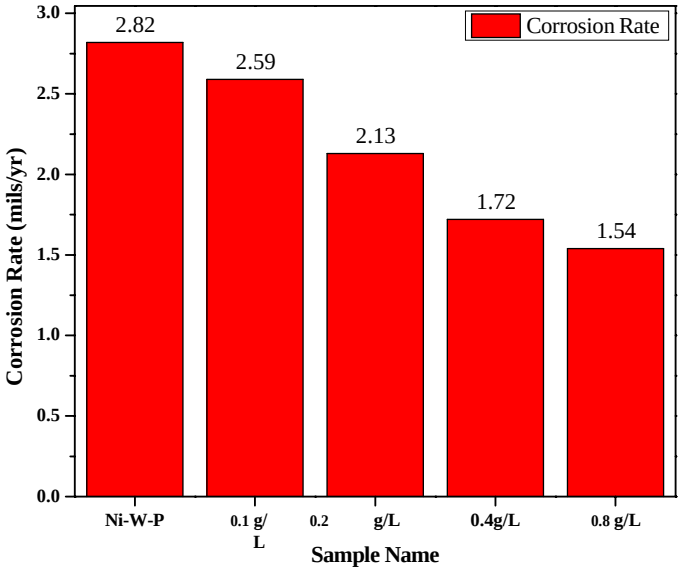

Figure 4.22. Comparison of corrosion rate values of HSLA steel substrate, Ni-W-P alloy and Ni-W-P/BN composite coatings with different BN concentrations. Corrosion rate decreases for each BN loading.

Table 4.9. Potentiodynamic polarization values for HSLA steel, Ni-W-P alloy, and Ni-W-P/ Al_2O_3 composite coatings.

Sample Name	I_{corr} **(A/cm^2)**	**Corrosion Rate (mils/yr)**
HSLA Steel	5.595×10^{-4}	41.09
Ni-W-P	3.840×10^{-5}	2.82
Ni-W-P/Al_2O_3 (0.1 g/L)	2.914×10^{-5}	2.14
Ni-W-P/Al_2O_3 (0.2 g/L)	1.078×10^{-5}	1.46
Ni-W-P/Al_2O_3 (0.4 g/L)	4.532×10^{-5}	3.32
Ni-W-P/Al_2O_3 (0.8 g/L)	5.665×10^{-5}	4.16

Table 4.10. Potentiodynamic polarization values for HSLA steel, Ni-W-P alloy, and Ni-W-P/BN composite coatings.

Sample Name	I_{corr} **(A/cm^2)**	**Corrosion Rate (mils/yr)**
HSLA Steel	5.595×10^{-4}	41.09
Ni-W-P	3.840×10^{-5}	2.82
Ni-W-P/BN (0.1 g/L)	3.524×10^{-5}	2.59
Ni-W-P/ BN (0.2 g/L)	2.907×10^{-5}	2.13
Ni-W-P/ BN (0.4 g/L)	2.347×10^{-5}	1.72
Ni-W-P/ BN (0.8 g/L)	2.103×10^{-5}	1.54

Conclusion and Future Work

Conclusions

- Ni-W-P alloy, Ni-W-P/Al_2O_3 and Ni-W-P/BN composite coatings were successfully deposited on HSLA steel substrate with good adhesion with HSLA substrate having the average coating thickness of 44.337 µm.
- Alloy and all Ni-W-P/Al_2O_3 and Ni-W-P/BN composite coatings were compact and crackles. They possessed lamellar structure which was well adhered to the HSLA steel substrate. It was noted that the Ni-W-P/Al_2O_3 composite coating was porosity free with 0.2g/L alumina inclusion and in Ni-W-P/BN composite coatings, 0.4 and 0.8g/L coatings are porosity free.
- SEM images revealed the nodular morphology of the alloy coatings and with the inclusion of alumina particles, nodules became finer (Al_2O_3-0.2g/L and BN coatings) which had a significant impact on mechanical properties of the coatings. With further increase in alumina and BN particles concentration, the agglomeration occurred.
- From AFM results, it was perceived that the roughness of the composite coatings increases continuously for both reinforcements. For 0.2g/L alumina and 0.8g/L BN, the roughness values were recorded as 6.22 nm and 82.4 nm respectively.
- Nano-indentation results revealed that at first the hardness values of the composite coatings increased with the inclusion of alumina parties and reaches to its maximum value of 11.60 GPa for 0.2g/L and then it decreased. This was due to the non-uniformity and agglomeration of alumina particles formed with higher concentration of alumina. For BN inclusions the hardness values increases for each loading. It was concluded that Ni-W-P/ Al_2O_3 (0.2g/L) composite coating is **3.43%** harder than Ni-W-P/BN (0.8g/L) composite coating.
- Friction coefficient also decreases to the value of 0.2255 with a certain amount of alumina particles (0.2g/L) of the composite coating Ni-W-P/Al_2O_3 and hence has the lowest wear rate of 1.946×10^{-8} mm^3/m and is the most wear resistant coating. FC and wear rate for BN came out to be the lowest i.e. 0.0710 and 6.634×10^{-10} mm^3/m. Hence, the friction coefficient of Ni-W-P/BN (0.8g/L) composite coating

is **52.11%** less than Ni-W-P/ Al_2O_3 (0.2g/L) composite coating and The wear rate of Ni-W-P/BN (0.8g/L) composite coating is **93.51%** less than Ni-W-P/ Al_2O_3 (0.2g/L) composite coating.

- Through potentiodynamic plots, the i_{corr} was calculated and through this the corrosion rate of the coatings was determined. It was observed that the composite coating with 0.2g/L alumina particles was the most corrosion resistant coating and has the value of 1.46 mils/year. The I_{corr} and corrosion rate of Ni-W-P/ Al_2O_3 (0.2g/L) composite coating is **32.23%** and **2.67%** better than Ni-W-P/BN (0.8g/L) composite coating respectively. For all compositions of BN didn't show better corrosion resistance than alumina 0.2g/L inclusion.
- It was concluded that the composite coating with 0.2g/L alumina particles exhibited the optimum values for all the mechanical and corrosion resistant properties and BN 0.8g/L showed the optimum coating for the tribological purposes.

Future Work

In future, the alloy and composite coatings of Ni-W-P/Al_2O_3 and Ni-W-P/BN can be annealed above 550 °C and its effects can be studied on their morphologies, phase transformation, mechanical and corrosion resistant properties.

Anneal coatings at different temperatures and then its effects and relation on mechanical and corrosion resistant properties can be studied.

Use of different corrosive environment to check their behavior on corrosion performance of the coatings.

References

[1] Fontana, M.G. and N.D. Greene, *Corrosion engineering*. (2018): McGraw-hill.

[2] Balaraju, J., et al., *Studies on electroless Ni–W–P and Ni–W–Cu–P alloy coatings using chloride-based bath.* (2006). **200**(16-17): p. 4885-4890.

[3] Balaraju, J., et al., *Studies on electroless Ni–W–P and Ni–W–Cu–P alloy coatings using chloride-based bath.* Surface and Coatings Technology, (2006). **200**(16-17): p. 4885-4890.

[4] Akyol, A., et al., *A novel approach for wear and corrosion resistance in the electroless Ni-PW alloy with CNFs co-depositions.* (2018). **453**: p. 482-492.

[5] Palaniappa, M. and S.J.W. Seshadri, *Friction and wear behavior of electroless Ni–P and Ni–W–P alloy coatings.* (2008). **265**(5-6): p. 735-740.

[6] Brooman, E.W.J.M.F., *Corrosion performance of environmentally acceptable alternatives to cadmium and chromium coatings: Chromium—Part II.* (2000). **98**(8): p. 39-45.

[7] Pillai, A.M., et al., *Electrodeposited nickel–phosphorous (Ni–P) alloy coating: an in-depth study of its preparation, properties, and structural transitions.* (2012). **9**(6): p. 785-797.

[8] Akyol, A., et al., *A novel approach for wear and corrosion resistance in the electroless Ni-PW alloy with CNFs co-depositions.* Applied Surface Science, (2018). **453**: p. 482-492.

[9] Yu, J., et al., *Effects of Sodium Hypophosphite on the Behaviors of Electrodeposited NiWP Alloy Coatings.* Journal of Materials Engineering and Performance, (2017). **26**(8): p. 3915-3920.

[10] Oliveira, M.C.L.d., et al., *Influence of the tungsten content on surface properties of electroless Ni-WP coatings.* Materials Research, (2017). **21**.

[11] Du, N. and M. Pritzker, *Investigation of electroless plating of Ni–W–P alloy films.* Journal of applied electrochemistry, (2003). **33**(11): p. 1001-1009.

[12] Gao, Y., et al., *The influence of cobalt on the corrosion resistance and electromagnetic shielding of electroless Ni–Co–P deposits on Al substrate.* Applied Surface Science, (2007). **253**(24): p. 9470-9475.

[13] Tsai, Y.-Y., et al., *Thermal stability and mechanical properties of Ni–W–P electroless deposits.* Surface and Coatings Technology, (2001). **146**: p. 502-507.

[14] Lu, G. and G. Zangari, *Corrosion resistance of ternary Ni□ P based alloys in sulfuric acid solutions.* Electrochimica Acta, (2002). **47**(18): p. 2969-2979.

[15] Leon, O., M. Staia, and H. Hintermann, *Wear mechanism of Ni–P–BN (h) composite autocatalytic coatings.* Surface and Coatings Technology, (2005). **200**(5-6): p. 1825-1829.

[16] Alishahi, M., et al., *The effect of carbon nanotubes on the corrosion and tribological behavior of electroless Ni–P–CNT composite coating.* Applied Surface Science, (2012). **258**(7): p. 2439-2446.

[17] Jiaqiang, G., et al., *Electroless Ni–P–SiC composite coatings with superfine particles.* Surface and Coatings Technology, (2006). **200**(20-21): p. 5836-5842.

[18] Chen, W., W. Gao, and Y. He, *A novel electroless plating of Ni–P–TiO2 nano-composite coatings.* Surface and Coatings Technology, (2010). **204**(15): p. 2493-2498.

[19] Imran, M., et al., *Enhanced visible light photocatalytic activity of TiO2 co-doped with Fe, Co, and S for degradation of Cango red.* (2021). **255**: p. 119644.

[20] Musil, J. and J. Vlček, *Magnetron sputtering of hard nanocomposite coatings and their properties.* Surface and Coatings Technology, (2001). **142**: p. 557-566.

[21] Kim, J., et al., *Growth by molecular beam epitaxy and electrical characterization of Si- doped zinc blende GaN films deposited on β- SiC coated (001) Si substrates.* Applied physics letters, (1994). **65**(1): p. 91-93.

[22] Mo, J., et al., *Comparison of tribological behaviours of AlCrN and TiAlN coatings—Deposited by physical vapor deposition.* Wear, (2007). **263**(7-12): p. 1423-1429.

[23] Gordon, R., *Chemical vapor deposition of coatings on glass.* Journal of Non-Crystalline Solids, (1997). **218**: p. 81-91.

[24] Chen, H. and C. Ding, *Nanostructured zirconia coating prepared by atmospheric plasma spraying.* Surface and Coatings Technology, (2002). **150**(1): p. 31-36.

[25] Sidhu, T., S. Prakash, and R. Agrawal, *Studies on the properties of high-velocity oxy-fuel thermal spray coatings for higher temperature applications.* Materials Science, (2005). **41**(6): p. 805-823.

[26] Rodriguez, R.M.P., et al., *Comparison of aluminum coatings deposited by flame spray and by electric arc spray.* Surface and Coatings Technology, (2007). **202**(1): p. 172-179.

[27] Wang, D. and G.P. Bierwagen, *Sol–gel coatings on metals for corrosion protection.* Progress in organic coatings, (2009). **64**(4): p. 327-338.

[28] Rabizadeh, T. and S.R. Allahkaram, *Corrosion resistance enhancement of Ni–P electroless coatings by incorporation of nano-SiO2 particles.* Materials & Design, (2011). **32**(1): p. 133-138.

[29] Pillai, A.M., A. Rajendra, and A. Sharma, *Electrodeposited nickel–phosphorous (Ni–P) alloy coating: an in-depth study of its preparation, properties, and structural transitions.* Journal of Coatings Technology and Research, (2012). **9**(6): p. 785-797.

[30] El-Sherik, A. and U. Erb, *Synthesis of bulk nanocrystalline nickel by pulsed electrodeposition.* Journal of Materials Science, (1995). **30**(22): p. 5743-5749.

[31] Pollard, B., *Spot welding characteristics of HSLA steel for automotive applications.* Welding Journal, (1974). **53**(8): p. 343.

[32] Paules, J.R., *Developments in HSLA steel products.* JOM, (1991). **43**(1): p. 41-44.

[33] Mohan, S., V. Prakash, and J. Pathak, *Wear characteristics of HSLA steel.* Wear, (2002). **252**(1-2): p. 16-25.

[34] Mendoza, B.I., et al., *Dissimilar welding of superduplex stainless steel/HSLA steel for offshore applications joined by GTAW.* Engineering, (2010). **2**(07): p. 520.

[35] Munford, M.L., *André Avelino Pasa.* (2006).

[36] Balaji, R., *Preparation and Characterization of Electrodeposits from Methane Sulphonic Acid Bath.* (2014).

[37] Nur, U.S., K. Ying, and N. Khuan, *Electrodeposition: Principles, Applications and Methods.*

[38] Li, C.-q., et al., *Nickel electrodeposition from novel citrate bath.* Transactions of Nonferrous Metals Society of China, (2007). **17**(6): p. 1300-1306.

[39] Krishnaveni, K., T.S. Narayanan, and S. Seshadri, *Electroless Ni–B coatings: preparation and evaluation of hardness and wear resistance.* Surface and Coatings Technology, (2005). **190**(1): p. 115-121.

[40] Seo, M.H., et al., *Characteristics of Ni–P alloy electrodeposited from a sulfamate bath.* Surface and Coatings Technology, (2004). **176**(2): p. 135-140.

[41] Mroz, K., et al., *Ni-W electrodeposited coatings on low carbon steel substrate: fatigue observations.* Journal of materials engineering and performance, (2014). **23**(10): p. 3459-3466.

[42] Sharma, A., et al., *Correlation between crystallographic texture, microstructure and magnetic properties of pulse electrodeposited nanocrystalline Nickel–Cobalt alloys.* Journal of magnetism and magnetic materials, (2017). **434**: p. 68-77.

[43] Goranova, D., G. Avdeev, and R. Rashkov, *Electrodeposition and characterization of Ni–Cu alloys.* Surface and Coatings Technology, (2014). **240**: p. 204-210.

[44] Halim, J., et al., *Electrodeposition and characterization of nanocrystalline Ni-Mo catalysts for hydrogen production.* Journal of Nanomaterials, (2012). **2012**.

[45] Srinivasan, R. and G. Ramesh Bapu, *Effect of additives on electrodeposition of nickel from acetate bath: cyclic voltammetric study.* Transactions of the IMF, (2013). **91**(1): p. 52-56.

[46] Godon, A., et al., *Characterization of electrodeposited nickel coatings from sulphamate electrolyte without additive.* Materials characterization, (2011). **62**(2): p. 164-173.

[47] Salehikahrizsangi, P., et al., *Erosion-corrosion behavior of highly hydrophobic hierarchical nickel coatings.* Colloids and Surfaces A: Physicochemical and Engineering Aspects, (2018). **558**: p. 446-454.

[48] Bigos, A., et al., *Citrate-based baths for electrodeposition of nanocrystalline nickel coatings with enhanced hardness.* Journal of Alloys and Compounds, (2021). **850**: p. 156857.

[49] Makhlouf, A., *Current and advanced coating technologies for industrial applications*, in *Nanocoatings and ultra-thin films*. (2011), Elsevier. p. 3-23.

[50] Wright, M.D., et al., *SAO/NASA ADS (null) Abstract Service.*

[51] Li, L. and S. Tin, *Effect of phosphorus content and grain size on the long-term phase stability of Ni-base superalloys.* Journal of Alloys and Compounds, (2020). **829**: p. 154352.

[52] Roy, S. and P. Sahoo. *ELECTROLESS Ni–P–W COATING: PREPARATION AND CHARACTERIZATION*. in *International Conference on Mechanical Engineering*. (2011).

[53] Biswas, A., S.K. Das, and P. Sahoo, *Investigation of the tribological behavior of electroless Ni-WP coating pre and post phase transformation regime.* Materials Research Express, (2019). **6**(9): p. 0965c1.

[54] Duari, S., et al., *Study of wear and friction of chemically deposited Ni-PW coating under dry and lubricated condition.* Surfaces and Interfaces, (2017). **6**: p. 177-189.

[55] Karunakaran, M., et al., *Electrodeposition of Cu-Ni-PW Composite on Al-6063 Substrate*. (2018).

[56] Oliveira, A.L.M., et al., *Studies on electrodeposition and characterization of the Ni–W–Fe alloys coatings.* Journal of Alloys and Compounds, (2015). **619**: p. 697-703.

[57] Wang, H., et al., *Effect of heat treatment on properties of Ni–Sn–P coatings.* Surface Engineering, (2018). **34**(6): p. 468-474.

[58] Yamasaki, T., et al., *Formation of amorphous electrodeposited Ni-W alloys and their nanocrystallization.* Nanostructured Materials, (1998). **10**(3): p. 375-388.

[59] Suvorov, D.V., et al., *Electrochemical deposition of Ni–W crack-free coatings.* Coatings, (2018). **8**(7): p. 233.

[60] Ko, Y.K., G.H. Chang, and J.H. Lee. *Nickel tungsten alloy electroplating for the high wear resistant materials applications*. in *Solid State Phenomena*. (2007). Trans Tech Publ.

[61] Jeong, D., et al., *The relationship between hardness and abrasive wear resistance of electrodeposited nanocrystalline Ni–P coatings.* Scripta Materialia, (2003). **48**(8): p. 1067-1072.

[62] Morikawa, T., et al., *Electrodeposition of Ni□ P alloys from Ni-citrate bath.* Electrochimica acta, (1997). **42**(1): p. 115-118.

[63] Wang, Y., et al., *Influence of pretreatments on physicochemical properties of Ni-P coatings electrodeposited on aluminum alloy.* Materials & Design, (2021). **197**: p. 109233.

[64] Balaraju, J. and K. Rajam, *Electroless deposition of Ni–Cu–P, Ni–W–P and Ni–W–Cu–P alloys.* Surface and coatings technology, (2005). **195**(2-3): p. 154-161.

[65] Duari, S., et al., *Study of wear and friction of chemically deposited Ni-PW coating under dry and lubricated condition.* (2017). **6**: p. 177-189.

[66] Yan, M., et al., *Improved microhardness and wear resistance of the as-deposited electroless Ni–P coating.* (2008). **202**(24): p. 5909-5913.

[67] Hsu, C.-I., et al., *The effect of incorporated self-lubricated BN (h) particles on the tribological properties of Ni–P/BN (h) composite coatings.* (2015). **357**: p. 1727-1735.

[68] Safavi, M., A. Rasooli, and F.J.T.o.t.I. Sorkhabi, *Electrodeposition of Ni-P/Ni-Co-Al2O3 duplex nanocomposite coatings: towards improved mechanical and corrosion properties.* (2020). **98**(6): p. 320-327.

[69] Biswas, A., S.K. Das, and P. Sahoo. *Hardness, Friction and Wear Trends of Electroless Ni-WP Coating Heat-Treated at Different Temperatures*. in *International Conference on Mechanical Engineering*. (2018). Springer.